

The Real Topological Vertex at Work

Daniel Krefl^a, Sara Pasquetti^b and Johannes Walcher^b

^a *IPMU, The University of Tokyo, Kashiwa, Japan*

^b *PH-TH Division, CERN, Geneva, Switzerland*

Abstract

We develop the real vertex formalism for the computation of the topological string partition function with D-branes and O-planes at the fixed point locus of an anti-holomorphic involution acting non-trivially on the toric diagram of any local toric Calabi-Yau manifold. Our results cover in particular the real vertex with non-trivial fixed leg. We give a careful derivation of the relevant ingredients using duality with Chern-Simons theory on orbifolds. We show that the real vertex can also be interpreted in terms of a statistical model of symmetric crystal melting. Using this latter connection, we also assess the constant map contribution in Calabi-Yau orientifold models. We find that there are no perturbative contributions beyond one-loop, but a non-trivial sum over non-perturbative sectors, which we compare with the non-perturbative contribution to the closed string expansion.

September 2009

Contents

1	Introduction	3
2	Classification of toric orientifolds	4
2.1	Anti-holomorphic involutions from symmetries of the toric diagram . . .	4
2.2	Geometric transitions	6
3	The real topological vertex	8
3.1	Conifold	9
3.2	The general case	12
3.3	A global sign rule	15
4	Chern-Simons	16
4.1	Review of ordinary vertex	16
4.2	Hořava operators	19
4.3	Derivation of the real vertex	21
5	Melting crystal	25
5.1	Melting crystal interpretation of the real vertex	26
5.2	Constant map contribution in orientifolds	29
6	Examples	34
6.1	Butterfly	35
6.2	Hybridfly	40
6.3	Pentafly	43
7	Conclusions	48
	Acknowledgments	49
	A Real Gopakumar-Vafa invariants	50
	References	57

1 Introduction

The topological vertex [1] provides a complete solution of the topological string on local toric Calabi-Yau manifolds. By conception, the vertex is an *open string* amplitude. However, the relevant D-branes (external, non-compact, toric branes) live in the realm of large- N duality, and can therefore be absorbed in the geometry by appropriate geometric transitions. This is indeed how the topological vertex was originally derived, and for this reason, it is most naturally used for the computation of *closed string* amplitudes.

It is a natural question to ask for extensions of the vertex formalism to situations involving D-branes that are not necessarily amenable to large- N duality. Two of the phenomena not covered by the standard formalism are boundary condition changing open strings (which are non toric) and the generation of a topological tadpole (toric branes only have a large- N limit because they do not generate such tadpoles). Concerning the second point, it was recently found in [2] that the partition function of the real topological string (namely, with D-branes and O-planes at the fixed point locus of an anti-holomorphic involution [3]) on local \mathbb{P}^2 indeed does admit a representation in the topological vertex formalism. (For previous studies of toric orientifolds after the topological vertex, see [4, 5]. For recent discussions of tadpole cancellation in topological strings and their orientifolds, see [6, 7].) The key new ingredient is a real version (as a kind of squareroot) of the topological vertex. Several questions were however not addressed in [2], and the purpose of the present work is to close these gaps.

We begin in section 2 with reviewing some general aspects of toric orientifold geometries. Considerations of the conifold will then be enough to obtain most of the real vertex formalism in section 3. The subtler aspects are several new sign rules, which we state in section 3, and justify in the remaining sections by comparison with Chern-Simons theory, examples, as well as global consistency conditions of the physical interpretation.

In section 4, we turn to the derivation of the real topological vertex from Chern-Simons theory. The relevant orientifold of the deformed conifold acts on the base S^3 with a fixed point locus in codimension 2. For the evaluation of these amplitudes, we will rely on some old work of Hořava [8].

In section 5, we study the real vertex from the point of view of the statistical model of melting crystal introduced in [9]. We show that the real vertex amplitude (at least

in case of trivial fixed leg) precisely computes the partition function of melting crystal configurations that are invariant under the exchange of two of the axes. (More precisely, as we will see in section 3, the real vertex actually comes in two versions. Both of them have a melting crystal interpretation.) In particular, in analogy with the MacMahon function, which is the counting function for plane partitions, capturing the constant map contribution of the topological string, we propose that the counting function for symmetric plane partitions (the “real” MacMahon function), encodes the constant map contribution of general Calabi-Yau orientifolds. A perhaps soothing consequence of this conjecture is that the constant map sector receives perturbative contributions from open and non-orientable worldsheets only at tree and one-loop level. The remainder of the real MacMahon function is non-perturbative in the string coupling.

We end in section 6 with some explicit examples, before concluding in section 7.

2 Classification of toric orientifolds

We are interested in orientifold models of A-type topological strings on a local toric Calabi-Yau manifold X . We intend to wrap our D-branes, which are necessary for tadpole cancellation, on top of the orientifold plane. Thus, to specify our model, all we need to do is identify a suitable anti-holomorphic involution $\sigma : X \rightarrow X$. Here we have in mind that the involution should be compatible with the toric symmetries of X so that we could in principle use localization techniques to compute A-model invariants, and ultimately will be able to compute using the (real) topological vertex formalism. The complete specification of the background includes of course also the closed and open string moduli, which is a point to which we will return in section 3.

2.1 Anti-holomorphic involutions from symmetries of the toric diagram

One way to identify suitable anti-holomorphic involutions is to use the gauged linear sigma model description of toric manifolds. Let’s have $N + 3$ chiral fields z_i , $i = 1, \dots, N + 3$, with charges Q_i^A (of $\sum_i Q_i^A = 0$) under the $U(1)^N$ gauge group with Fayet-Iliopoulos (FI) parameters t^A , $A = 1, \dots, N$. In the absence of a GLSM superpotential (toric Calabi-Yaus are always rigid), one anti-holomorphic involution that always exists is simply conjugating all fields $\sigma_0 : z_i \rightarrow \bar{z}_i$. Other involutions can be obtained by dressing this basic involution with global (holomorphic) symmetries g of the model, such that the dressed involution $\sigma_g = g \circ \sigma_0$ is still involutive. This means

that $(\sigma_g)^2$ is equivalent to the identity modulo a $U(1)^N$ gauge transformation. Typical symmetries g one can consider include permutations of variables (possibly combined with permutations of the gauge group factors), as well as phase rotations on the variables. Note that dressings that can be related to each other by conjugating σ_g with a global symmetry should be considered equivalent. (This is not the same as conjugating g !) We will see these options at work in examples below, but otherwise shall not develop the GLSM point of view any further here.

For purposes of the topological vertex, as explained in [1], we think of our toric manifold X in terms of a certain $T^2 \times \mathbb{R}$ -fibration over a three-dimensional base. This three-dimensional base is the image of X under the “moment maps”

$$r_\alpha = |z_1|^2 - |z_3|^2, \quad r_\beta = |z_2|^2 - |z_3|^2, \quad r_\gamma = \text{Im}(\prod_i z_i) \quad (2.1)$$

(where we have arbitrarily distinguished the first three fields), and the $T^2 \times \mathbb{R}$ fibers are the orbits of the Hamiltonian flows generated by $r_\alpha, r_\beta, r_\gamma$ with respect to the symplectic form $\omega = \sum_i dz_i \wedge d\bar{z}_i$, modulo symplectic reduction to $\sum Q_i^A |z_i|^2 = t^A$. The T^2 fibers degenerate over a certain piecewise linear trivalent graph Γ in the r_α - r_β plane, known as the toric, or (p, q) -web, diagram. (For full details, see [1].)

The anti-holomorphic involutions of our interest can be described in terms of their action on this toric diagram. (As we will see below, the topological vertex formalism does not distinguish between different dressing phases, which lead to different actions on the T^2 fibers.) Essentially, σ acts as a linear involution on the r_α - r_β plane and induces a symmetry of X if it maps the toric diagram to itself. Now note that since $\sigma(\omega) = -\omega$, the isometries of T^2 compatible with the involution are generated by eigenvectors of σ with eigenvalue -1 . In particular, the trivial action on Γ does not preserve any symmetries¹, which is not enough for our purposes. This leaves two possibilities. When σ acts with two negative eigenvalues, we are dealing with a “point reflection”. By an appropriate choice of phases, one can arrange that σ acts without fixed points on the total space of the fibration, which is our Calabi-Yau X . Thus, the orientifold plane is empty, and we should not wrap any D-brane for tadpole cancellation. The implementation of this situation at the level of the topological vertex was studied in detail in [4], and will be subsummed in our formalism below. The last possibility is that σ acts in the r_α - r_β plane with eigenvalues $(+1, -1)$. This corresponds to “reflection

¹There are cases, such as the conifold, where the trivial involution preserves additional accidental $U(1)$ symmetries. There is then a different presentation of the manifold which makes this manifest.

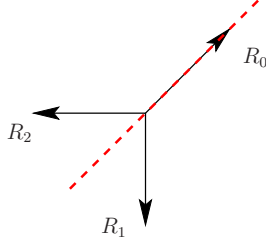


Figure 1: The local geometry around a fixed vertex is \mathbb{C}^3 with involution acting as $(z_0, z_1, z_2) \rightarrow (\bar{z}_0, \bar{z}_2, \bar{z}_1)$. The R_i denote the $U(\infty)$ representations propagating on the legs in the topological vertex formalism. Invariance under the involution requires $R_0 = R_0^t$, and $R_2 = R_1^t$.

at a line". In that case, the action of σ on X will typically have fixed points, and we should wrap D-branes on top of these orientifold planes.

The line reflection is the richest of these possibilities. Consider in particular the intersection of the fixed line in the r_α - r_β plane with the toric diagram Γ . The finite legs of Γ that are fixed under the involution fall in two classes. They can either intersect the fixed line perpendicularly (which we will call fixed legs of type 2) or be fixed point-wise (type 3). (The fixed legs that can occur in the point reflection we refer to as of type 1.) Fixed legs of type 3 end in two fixed vertices, around which the local geometry is as depicted in figure 1. This is the geometry that necessitates the real topological vertex.

2.2 Geometric transitions

It is instructive and useful for the subsequent Chern-Simons discussion to review here the possible A-type orientifolds of the conifold, their toric realization, and their relation under the conifold transition.

Recall first (see, *e.g.*, [10]) the classification of anti-holomorphic involutions of the resolved and deformed conifold as Kähler manifolds (forgetting the torus action). On the resolved side, the possible involutions are distinguished by the action on the base \mathbb{P}^1 of $\mathcal{O}(-1) \oplus \mathcal{O}(-1)$. Namely, this action can be fixed point free, $z \rightarrow -1/\bar{z}$, where z is an inhomogeneous coordinate on \mathbb{P}^1 , or the fixed point locus is an S^1 , $z \rightarrow 1/\bar{z}$. The deformed conifold, T^*S^3 can be thought of as the hypersurface $\sum x_i^2 = \mu$ in \mathbb{C}^4 . Fixing an anti-holomorphic involution imposes a reality condition on the deformation



Figure 2: Left: (p, q) -web of the resolved conifold. The z_i indicate which coordinate vanishes on the corresponding toric divisor. Right: Illustration of the three involutive symmetries of the web diagram.

parameter μ . The topological type of the fixed point locus depends on the signs in $\sum \pm x_i^2 = \mu$, with all variables real. When all signs are $+1$, the fixed point locus is S^3 for $\mu > 0$, and empty for $\mu < 0$. Under conifold transition, this is related to the fixed point free action on the resolved conifold. For an odd number of -1 's, the fixed point locus is $S^2 \times \mathbb{R}$ or $\mathbb{R}^3 \cup \mathbb{R}^3$ (depending on the sign of μ). This involution is not compatible with the small resolution as the Kähler deformation at $\mu = 0$ is projected out. Finally, for two $+1$'s and two -1 's, the fixed point locus is $S^1 \times \mathbb{R}^2$, and this is related to the involution of the resolved conifold whose fixed locus is also $S^1 \times \mathbb{R}^2$.

We now describe how these involutions are realized at the level of the toric geometry. The web diagram of the resolved conifold is shown in figure 2. It has three apparent non-trivial symmetries: A point reflection at the center of the compact edge (we refer to this as involution 1), a reflection at a line perpendicular to the compact leg (involution 2), and a reflection at the line containing the compact leg (involution 3). To understand the corresponding fixed point loci, we lift the action to the fields of the GLSM: (z_1, z_2, z_3, z_4) , of charge $(1, 1, -1, -1)$, with FI $t > 0$. We deduce that involution 2 acts by $(z_1, z_2, z_3, z_4) \rightarrow (\bar{z}_2, \bar{z}_1, \bar{z}_3, \bar{z}_4)$, while involution 3 sends (z_1, z_2, z_3, z_4) to $(\bar{z}_1, \bar{z}_2, \bar{z}_4, \bar{z}_3)$ (up to conjugation by global symmetries). Those two involutions are related by a flop, see figure 3 on page 11 and the fixed point locus on \mathbb{P}^1 is S^1 . (The full O-plane has topology $S^1 \times \mathbb{R}^2$.) Turning to involution 1, complex conjugation must be dressed by exchanging both, z_1, z_2 and z_3, z_4 . In addition, we can allow for a non-trivial phase dressing. Namely, we have the two possible lifts: $(z_1, z_2, z_3, z_4) \rightarrow (\bar{z}_2, \bar{z}_1, \bar{z}_4, \bar{z}_3)$

and $(z_1, z_2, z_3, z_4) \rightarrow (\bar{z}_2, -\bar{z}_1, \bar{z}_4, -\bar{z}_3)$. (The point being that the second involution squares to $(-1, -1, -1, -1)$, which is gauge equivalent to the identity.) The fixed point locus for the first choice is S^1 , in the second the action is fixed point free.

3 The real topological vertex

The topological vertex formalism computes the A-model topological string partition function Z_X of a toric Calabi-Yau manifold X from the toric diagram Γ . Orient each compact leg of the toric diagram, and attach a Young diagram R_i , $i = 1, \dots, l$. Then Z_X is obtained by summing over the R_i a certain rational function $P_{(R_i)}(q, Q_A)$ of $N + 1$ variables (one, $Q_A = e^{-t_A}$, for each Kähler class, and one, $q = e^{g_s}$, for the string coupling) constructed from contributions at each vertex and each compact leg.

$$Z_X(q, Q_A) = \sum_{(R_i)} P_{(R_i)}(q, Q_A). \quad (3.1)$$

As explained in [2], the basic idea behind the real topological vertex is that the action of the involution on Γ induces a symmetry of the sum over R_i 's. The terms fixed under the involution are, appropriately interpreted, perfect squares when the parameters Q_A are also appropriately restricted, $\sigma(Q_A) = Q_A$, and the real topological string partition function of X with involution σ , is given by

$$Z_X^\sigma = \sum_{(R_i)=\sigma(R_i)} \pm \sqrt{P_{(R_i)}}. \quad (3.2)$$

Really, the real topological vertex is the theory of signs in taking this squareroot. To isolate the genuine open+unoriented contribution, we reduce with respect to the closed string partition function,

$$Z_X'^\sigma = \frac{Z_X^\sigma}{\sqrt{Z_X}}, \quad (3.3)$$

such that the (reduced) real topological string free energy reads

$$\mathcal{G}_X'^\sigma = \log(Z_X'^\sigma). \quad (3.4)$$

Note that the restriction on the Q_A is the usual orientifold projection of Kähler parameters. Taking the squareroot of $P_{(R_i)}$ often also involves a squareroot of some of the Q_A . The resulting sign degree of freedom can usually be interpreted as a discrete Wilson line on the D-brane wrapped around the corresponding component of the fixed point locus, *i.e.*, as a discrete open string modulus.

3.1 Conifold

Let us see how this procedure works for the involutions of the conifold described in the previous section. The closed topological string partition function is in the topological vertex formalism computed as

$$Z_{\text{con.}}(q, Q) = \sum_R (-1)^{\ell(R)} Q^{\ell(R)} C_{..R}(q) C_{..R^t}(q). \quad (3.5)$$

Here, $Q = e^{-t}$ is the single Kähler parameter of the geometry, $q = e^{g_s}$ with g_s the topological string coupling. The sum runs over all partitions $R = (\lambda_1, \lambda_2, \dots)$ with number of boxes computed by $\ell(R) = \sum \lambda_i$. $C_{..R}(q)$ is the 1-legged topological vertex, which can be expressed in terms of the standard Schur function

$$C_{..R}(q) = s_R(q^\rho). \quad (3.6)$$

(The notation means evaluating s_R at $x_i = q^{-i+1/2}$, for $i = 1, 2, \dots$) Using the elementary Schur function identity

$$\sum_R s_R(x) s_{R^t}(y) = \prod_{i,j=1}^{\infty} (1 + x_i y_j), \quad (3.7)$$

we obtain the standard expression [11] for Z ,

$$Z_{\text{con.}}(q, Q) = \prod_{n=0}^{\infty} (1 - Q q^{-n})^n = \exp\left(-\sum_{k=1}^{\infty} \frac{Q^k}{k(q^{k/2} - q^{-k/2})^2}\right). \quad (3.8)$$

Involution 1

The point reflection acts on the summation variable in (3.5) by $R \rightarrow R^t$. The sign of the squareroot of the fixed configurations has been found in [4] to be determined by the *rank* of the corresponding self-conjugate representation, *i.e.*, the number of boxes on the diagonal

$$r(R) = \#\{\lambda_i \geq i\}. \quad (3.9)$$

Occasionally, we will refer to this sign as an “ r -type sign”. We obtain

$$Z_{\text{con.}}^1 = \sum_{R=R^t} (-1)^{(\ell(R) \mp r(R))/2} Q^{\ell(R)/2} C_{..R}(q). \quad (3.10)$$

Note that the sign of the squareroot $Q^{1/2}$ is equivalent to the sign ∓ 1 in front of $r(R)$. We can now use the Schur function identity [12]

$$\sum_{R=R^t} (-1)^{(\ell(R) \mp r(R))/2} s_R(x) = \prod_{i=1}^{\infty} (1 \pm x_i) \prod_{1 \leq i < j}^{\infty} (1 - x_i x_j), \quad (3.11)$$

to obtain the expression

$$Z_{\text{con.}}^1 = \exp\left(-\frac{1}{2} \sum_{k=1}^{\infty} \frac{Q^k}{k(q^{k/2} - q^{-k/2})^2} - \sum_{k=1}^{\infty} \frac{(\pm Q)^{k/2}}{k(q^{k/2} - q^{-k/2})}\right). \quad (3.12)$$

This is the expected result. It can be interpreted as the partition function of Chern-Simons theory on S^3 with orthogonal or symplectic gauge group, depending on the sign ± 1 , which is the sign of the crosscap amplitude in the topological string interpretation. This is consistent with the geometric transition to orientifold of deformed conifold with S^3 fixed locus, as was first observed in [13].

Involution 2

This involution leaves R in (3.5) invariant, so the summation variable is not restricted. To see that we nevertheless have a perfect square, we need to use the identity

$$s_{R^t}(q) = q^{-\kappa(R)/2} s_R(q), \quad (3.13)$$

where $\kappa(R) = \sum \lambda_i(\lambda_i - 2i + 1)$. The sign of the squareroot we can borrow from [2]. We denote the *number of boxes in even rows* by $p(R)$,

$$p(R) = \sum_i \lambda_{2i}. \quad (3.14)$$

Note that one may write

$$p(R) = (\ell(R) - c(R))/2, \quad (3.15)$$

where $c(R)$ is the *number of columns of odd height*. This is a quantity that features in section I.5 of [12], thus exhibiting the representation theoretic relevance of $p(R)$. Occasionally, we will refer to this sign as a “ c -type sign”. Note that as for the r -type sign, the c -type sign is itself only determined up to a sign, $(-1)^{\ell(R)}$. Namely, a replacement of $r(R)$ with $-r(R)$ can be absorbed in a corresponding open string degree of freedom (the sign of $Q^{1/2}$). We obtain

$$Z_{\text{con.}}^2 = \sum_R (-1)^{(\ell(R) \mp c(R))/2} Q^{\ell(R)/2} q^{-\kappa(R)/4} C_{..R}(q). \quad (3.16)$$

We have not been able to identify any Schur identity to sum this expression. But low degree expansion in Q reveals that in fact

$$Z_{\text{con.}}^2 = Z_{\text{con.}}^1. \quad (3.17)$$

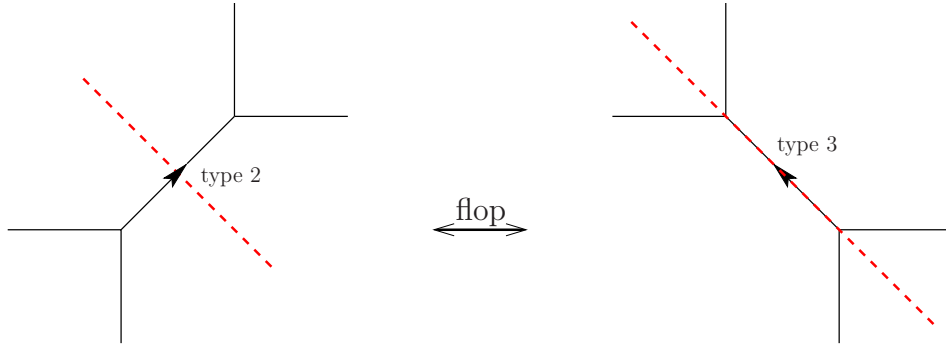


Figure 3: A flop of the resolved conifold relates the involutions with fixed leg of type 2 and type 3.

This is also the expected result: For involution 2 we need to wrap a D-brane on the fixed point locus, and the sign of the squareroot $Q^{1/2}$ is the value of the discrete Wilson line at the critical locus of the superpotential. (Going to this critical locus also eliminates any potential framing dependence.) The difference between involution 1 and involution 2 is merely whether we give a BPS/enumerative interpretation of the second term in the exponential of (3.12) as a crosscap or disk respectively.

Note that as for the r -type sign, the sign of $c(R)$ in the c -type sign is equivalent to the sign of the squareroot of $Q^{1/2}$. However, in contrast to the r -type sign, the c -type sign comes with an additional degree of freedom. Namely, we may as well have used $c(R^t)$, which is generally not equal to $c(R)$. For the conifold, the two possibilities yield the same result. However, for more complicated models taking account of this additional degree of freedom turns out to be crucial. We will come back to this point in the more general discussion below.

Involution 3

We expect this involution to also give the same result as involution 1 and 2 (after all, as a string background, this is identical to involution 2). Stated more generally, we expect that the flop invariance of the closed topological vertex carries over to orientifolds, as illustrated in figure 3. Especially, the flop transition transforms a type 2 fixed leg to a type 3 fixed leg and vice versa.

On the other hand, the naive application of the squareroot philosophy requires the real vertex with non-trivial fixed leg, in other words, the squareroot of $C_{..R}(q) = s_R(q^\rho)$.

However, recalling the formula

$$s_R(q^\rho) = q^{n(R)-l(R)/2} \prod_{(i,j) \in R} (1 - q^{h(i,j)})^{-1}, \quad (3.18)$$

with $n(R) = \sum_i (i-1)\lambda_i$ and $h(i,j)$ the Hook length $h(i,j) = 1 + \lambda_i + \lambda_j^t - i - j$, we see that $s_R(q)$ is *not* a perfect square even for $R = R^t$ (where only the terms on the diagonal, $i = j$, remain unpaired). This was pointed out in [2].

Thinking somewhat more generally about fixed vertices with non-trivial fixed leg in arbitrary toric diagrams, we notice that we can save the situation by exploiting the fact that such a fixed leg will always end on another fixed vertex. (Otherwise, the leg is external, and carries a trivial representation.) The two squareroots can be combined to a rational expression, and this is what we propose for fixed legs of type 3 in the general case. (More precisely, we will have to amend one additional sign in the real vertex, as compared with [2].)

Returning to involution 3 of the conifold, we use the same formulas and signs as for involution 1, and obtain trivially

$$Z_{\text{con.}}^3 = Z_{\text{con.}}^1, \quad (3.19)$$

as required.

3.2 The general case

We don't need to recall the full rules of the ordinary topological vertex formalism for computing the rational function $P_{(R_i)}(Q^A, q)$ in (3.1). It suffices to observe that the contributions from legs and vertices that are not fixed by the involution σ (and instead, are paired by it) automatically give rise to a perfect square when representations are restricted to the fixed configurations. In other words, this part of the amplitude is given by the ordinary vertex formalism, evaluated on the smooth part of the quotient of the toric diagram by σ . It remains to describe the contribution from legs and vertices that are fixed under σ . This is most easily done by considering the gluing of two vertices adjacent to a fixed leg, and then taking a squareroot. A special case of this is obtained by adding external representations to the involutions of the conifold described above.

In the usual vertex formalism, the gluing of two vertices along a common edge is given by

$$\sum_{R_i} C_{R_j R_k R_i} e^{-t_i \ell(R_i)} (-1)^{(n_i+1)\ell(R_i)} q^{-n_i \kappa_{R_i}/2} C_{R_i^t R_j^t R_k^t}. \quad (3.20)$$

Here, one is assuming that the edges decorated with R_j, R_k are outgoing in direction v_j, v_k at the first vertex, and the edges decorated with R'_j, R'_k are outgoing in direction v'_j, v'_k at the second vertex, respectively. The cycling ordering (with respect to some fixed orientation of the r_α - r_β plane) is as indicated on the C 's, which represent the topological vertex in canonical framing. Then n_i is the integer $n_i = v'_j \wedge v_j$ accounting for the adjustment of framing between the two vertices. Let us now describe the squareroot of this amplitude for the three types of fixed legs discussed at the end of section 2.

Fixed legs of type 1 (point reflection at the center of the line) were treated in [4]. Inspection shows that in this case, $v'_j = -v_j, v'_k = -v_k$, and hence $n_i = 0$. The restriction to invariant configurations of Young diagrams imposes $R_i = R_i^t, R'_j = R_j, R'_k = R_k$. The squareroot is

$$\sum_{R_i=R_i^t} e^{-t_i \ell(R_i)/2} (-1)^{(\ell(R_i) \pm r(R_i))/2} C_{R_j R_k R_i}, \quad (3.21)$$

where we inserted an r -type sign, as defined in (3.9).

For fixed legs of type 2, the j leg is mapped to the k' leg, and the k leg to the j' leg. Invariant configurations have $R'_k = R_j^t$ and $R'_j = R_k^t$, with no restriction on R_i . (Compared with type 1, there is an additional transposition because of the orientation reversal of the r_α - r_β plane.) The amplitude is then a sum of perfect squares because of the symmetry

$$C_{R_i^t R_k^t R_j^t} = q^{-\kappa_{R_i}/2 - \kappa_{R_j}/2 - \kappa_{R_k}/2} C_{R_i R_j R_k}, \quad (3.22)$$

of the topological vertex. The sign of the squareroot is in principle determined by the c -type sign defined around (3.14).

$$\sum_{R_i} e^{-t_i \ell(R_i)/2} (-1)^{(n_i+1)(\ell(R_i) \pm c(R_i))/2} q^{-(n_i+1)\kappa_{R_i}/4 - \kappa_{R_j}/4 - \kappa_{R_k}/4} C_{R_j R_k R_i}. \quad (3.23)$$

However, as alluded to above, it is necessary to allow for the replacement of $c(R_i)$ with $c(R_i^t)$ in this expression. The choice between the two options depends on a global consistency condition that we explain in subsection 3.3 below. We will corroborate this rule at hand of examples in section 6.

Finally, we discuss fixed legs of type 3. In that case, the invariant configurations have $R_j = R_k^t$, and $R'_j = R_k^t$. To find the squareroot of the resulting expression, we have to delve deeper into the structure of the topological vertex

$$C_{R_j R_k R_i} = q^{(\kappa_{R_i} + \kappa_{R_j})/2} \sum_{Q_j, Q_k, Q} N_{QQ^t}^{R_k} N_{QQ_j}^{R_j^t} \frac{W_{R_i^t Q_k^t} W_{R_i Q_j}}{W_{R_i}}. \quad (3.24)$$

We also recall that the real vertex was introduced in [2] as the squareroot of this expression for $R_k = R_j^t$, when the summand is almost a perfect square. As anticipated in the previous subsection, we deal with the non-trivial fixed leg, $R_i = R_j^t$, by simply taking the squareroot of the lone W_{R_i} in the denominator,

$$C_{R_j R_i}^{\text{real}} = q^{\kappa_{R_j}/4} \sum_{Q_j, Q} N_{QQ_j}^{R_j^t} \frac{W_{R_i Q_j}}{\sqrt{W_{R_i}}}, \quad (3.25)$$

and noting that the squareroots of the two real vertices recombine to give a rational function of q for the full contribution of a fixed leg of type 3.

Somewhat similarly to fixed legs of type 2, we have found that it is necessary to include an additional sign degree of freedom in the real vertex. Together with (3.25), which we'll call the "straight" real vertex, we define the "twisted" real vertex as

$$\tilde{C}_{R_j R_i}^{\text{real}} = q^{\kappa_{R_j}/4} \sum_{Q_j, Q} (-1)^{\ell(Q)} N_{QQ_j}^{R_j^t} \frac{W_{R_i Q_j}}{\sqrt{W_{R_i}}}. \quad (3.26)$$

According to the global sign rule which we explain below, the full contribution of a fixed leg of type 3 is then given by

$$\sum_{R_i=R_j^t} C_{R_j R_i}^{\text{real}} e^{-t_i \ell(R_i)/2} (-1)^{(\ell(R_i) \mp r(R_i))/2} \tilde{C}_{R_j R_i}^{\text{real}}. \quad (3.27)$$

For later reference, note that by using the expression of W in terms of Schur functions

$$W_{R_i Q_j} = s_{R_i}(q^\rho) s_{Q_j}(q^{R_i+\rho}), \quad (3.28)$$

with $q^{\rho+R_j} = (q^{R_j^1-1/2}, q^{R_j^2-3/2}, \dots)$, where R_j^i denotes the i -th part of the partition R_j , and the expression $s_{\lambda/\mu}(x) = \sum_\nu N_{\mu\nu}^\lambda s_\nu(x)$ for skew Schur functions, the untwisted (3.25) and twisted (3.26) real vertex can be expressed in terms of Schur functions as

$$C_{R_j R_i}^{\text{real}} = q^{\kappa_{R_j}/4} \sqrt{s_{R_i}(q^\rho)} \sum_Q s_{R_j^t/Q}(q^{\rho+R_i}), \quad (3.29)$$

and

$$\tilde{C}_{R_j R_i}^{\text{real}} = q^{\kappa_{R_j}/4} \sqrt{s_{R_i}(q^\rho)} \sum_Q (-1)^{\ell(Q)} s_{R_j^t/Q}(q^{\rho+R_i}). \quad (3.30)$$

respectively. Note that (3.29) is, as expected, just a termwise squareroot of the full topological vertex expressed in Schur functions (*cf.*, [1]).

3.3 A global sign rule

To complete the real vertex formalism, we need to specify how to correlate the choice between $c(R)$ and $c(R^t)$ on fixed legs of type 2 with the choice between straight and twisted real vertex at the ends of fixed legs of type 3. As is not uncommon for orientifolds, this is a non-local issue, *i.e.*, not every combination is globally consistent. Note that the question only arises when the involution changes the orientation of the plane (otherwise all fixed legs are of type 1). The fixed line of this involution then divides the r_α - r_β -plane of the toric diagram in two parts, which we choose to call “above the fixed line” and “below the fixed line”, respectively. This then also determines a left-right orientation of the fixed line itself.

In the topological vertex, one has to take account of the cyclic ordering of the outgoing legs. We work in conventions in which $C_{R_0 R_1 R_2}$ is the amplitude when the representations R_0 , R_1 , and R_2 appear in clockwise order. (See figure 1.) The real vertex is the squareroot of this amplitude when $R_0 = R_0^t$ and $R_2 = R_1^t$, and we label it by R_0 and R_1 , which is the representation following the fixed leg in clockwise direction. The choice between straight (3.25) and twisted (3.26) real vertex now depends on the orientation of the fixed vertex relative to the chosen orientation of the r_α - r_β -plane: When the fixed leg points to the left, we use $C_{R_1 R_0}^{\text{real}}$, and when it points to the right, we use $\tilde{C}_{R_1 R_0}^{\text{real}}$. Note that this implies that in the former case, the leg carrying R_1 lies above the fixed line, while in the latter case, it lies below the fixed line.

For fixed legs of type 2, we use $c(R)$ when the leg crosses the fixed line from above, and we use $c(R^t)$ when it crosses from below.

We emphasize that in this prescription, every word counts. Once the orientations are fixed, we could make one global choice:² Whether to use C^{real} or \tilde{C}^{real} for fixed legs pointing left. The opposite choice (*i.e.*, \tilde{C}^{real} for fixed legs pointing left, C^{real} for those pointing right, $c(R^t)$ for legs crossing from above, and $c(R)$ for those crossing from below) also gives a consistent theory, although the sign of some (real Gopakumar-Vafa) invariants might change. (The choice of sign in front of $r(R)$ and $c(R)$ also changes the sign of these invariants, but as emphasized before, this can be absorbed in the discrete Wilson lines.)

To illustrate the rule, we consider local \mathbb{P}^2 in the real vertex formalism, see figure 4. Evaluation of the rule above gives for the diagram on the left,

²There are geometries for which accidentally more choices are possible, but the rule as we have stated it is the only globally consistent one.

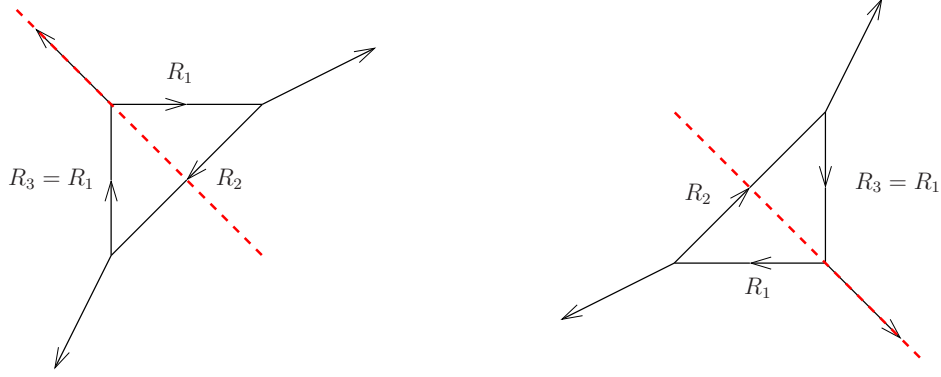


Figure 4: Two web diagrams of local \mathbb{P}^2 with involution with different orientation for purposes of the real vertex.

$$\sum_{R_1 R_2} (-1)^{\ell(R_1) + (\ell(R_2) - c(R_2))/2} q^{5\kappa_{R_1}/4 + \kappa_{R_2}/4} e^{-t(\ell(R_1) + \ell(R_2)/2)} C_{R_1}^{\text{real}} C_{R_1^t \cdot R_2}, \quad (3.31)$$

and for that on the right

$$\sum_{R_1 R_2} (-1)^{\ell(R_1) + (\ell(R_2) - c(R_2^t))/2} q^{5\kappa_{R_1}/4 + \kappa_{R_2}/4} e^{-t(\ell(R_1) + \ell(R_2)/2)} \tilde{C}_{R_1}^{\text{real}} C_{R_1^t \cdot R_2}. \quad (3.32)$$

One may check that (3.31) and (3.32) give the same result for the real topological string partition function of local \mathbb{P}^2 .

4 Chern-Simons

The ordinary topologically vertex was originally derived in [1] by exploiting the duality between topological strings on resolved conifold with external branes and Chern-Simons theory with Wilson loop insertions. The purpose of the present section is to give a similar derivation of the real vertex, which we have obtained in the previous section as the squareroot of the ordinary vertex. Let us first give a brief review of the derivation of [1].

4.1 Review of ordinary vertex

The derivation of the topological vertex begins with the conifold geometry with three toric Lagrangian branes inserted as probes, in a configuration sketched in figure 5.

This amplitude is evaluated in the Chern-Simons description, as we will review below. The vertex itself, which corresponds to the brane configuration in \mathbb{C}^3 depicted

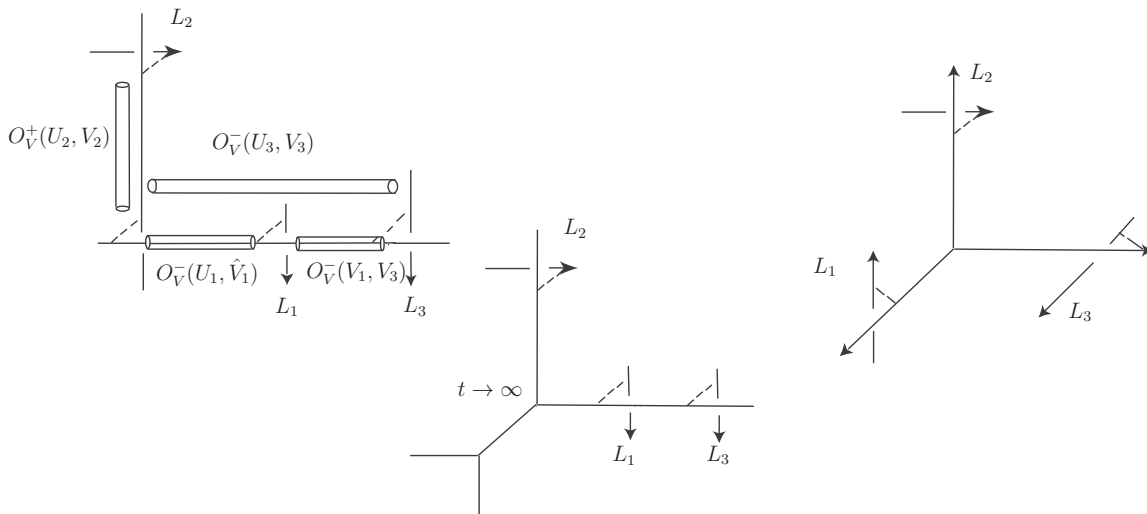


Figure 5: The D-brane configuration used by [1] for the derivation of the topological vertex.

in figure 5 on the right, is obtained by first taking the Kähler parameter of the conifold $t \rightarrow \infty$, to obtain the configuration in the middle of figure 5, and then moving the Lagrangian brane L_1 to the third outgoing edge and adjusting framing.

The role of the probe branes in the topological vertex formalism is to “cut” the toric diagram of a toric Calabi-Yau threefold into \mathbb{C}^3 -patches. This cutting procedure requires for each brane the choice of a framing, depicted in figure 5 by arrows (as well as an additional subtlety, recorded below).

The probe branes couple to the Chern-Simons theory via annulus worldsheets, also depicted in figure 5. The net effect of these annuli is the insertion of a certain Wilson line, known as the Ooguri-Vafa operator, into the Chern-Simons path integral. More precisely, the Ooguri-Vafa operator comes in two guises, depending on whether the branes connected by the annulus lie on opposite or the same sides of the corresponding lines of the toric diagram:

$$\begin{aligned}
 O_V^+(U, V) &= \sum_Q \text{Tr}_Q U e^{-r\ell(Q)} \text{Tr}_Q V, \\
 O_V^-(U, V) &= \sum_Q \text{Tr}_Q U e^{-r\ell(Q)} (-1)^{\ell(Q)} \text{Tr}_Q V.
 \end{aligned}
 \tag{4.1}$$

Here, U , and V are the holonomies of the D-brane gauge field around the two ends of the cylinder, r is its length, and the sums are over all $U(\infty)$ representations. In the

above configuration, we have the four Ooguri-Vafa operators,

$$O_V^-(U_1, \widehat{V}_1), \quad O_V^+(U_2, V_2), \quad O_V^-(U_3, V_3), \quad O_V^-(V_1, V_3). \quad (4.2)$$

On the dynamical branes the Wilson lines U_1 and U_3 are parallel and form with U_2 a double Hopf link whose normalized Chern-Simons expectation value is given by

$$\frac{\langle \text{Tr}_{Q_1^t} U_1 \text{Tr}_{Q_3^t} U_1 \text{Tr}_{Q_2} U_2 \rangle}{\langle \cdot \rangle} = \frac{\mathcal{W}_{Q_1^t Q_2} \mathcal{W}_{Q_3^t Q_2}}{\mathcal{W}_{Q_2}}, \quad (4.3)$$

where $\mathcal{W}_{R_1 R_2} = S_{R_1 R_2} / S_{00}$ is the Hopf link invariant and $S_{R_1 R_2}$ is the modular S-matrix of the relevant WZW-model.³ We also recall the relations

$$g_s = \frac{2\pi i}{k + N}, \quad t = N g_s, \quad (4.4)$$

between topological string coupling g_s , Kähler parameter t , and Chern-Simons parameters rank, N , and level, k . In the limit of interest, $t \rightarrow \infty$, one defines

$$W_{R_1 R_2} = \lim_{t \rightarrow \infty} e^{-\frac{\ell(R_1) + \ell(R_2)}{2} t} \mathcal{W}_{R_1 R_2}, \quad (4.5)$$

and this yields for the configuration in the middle of figure 5:⁴

$$\sum_{Q_1, Q_2, Q_3, Q} (-1)^{\ell(Q_1) + \ell(Q_2) + \ell(Q_3)} \frac{W_{Q_1^t Q_2} W_{Q_3^t Q_2}}{W_{Q_2}} \text{Tr}_{Q_1} \widehat{V}_1 \text{Tr}_{Q^t} V_1 \text{Tr}_{Q_2} V_2 \text{Tr}_Q V_3 \text{Tr}_{Q_3} V_3. \quad (4.6)$$

By considering the simplified situation with only branes L_1 and L_2 present, and exploiting symmetries of the vertex, one finds that moving L_1 to the empty leg amounts to replacing $(-1)^{\ell(Q_1)} W_{Q_1^t Q_2} \text{Tr}_{Q_1} \widehat{V}_1 \text{Tr}_{Q_2} V_2$ with $(-1)^{\ell(Q_2)} q^{\kappa_{Q_2}/2} W_{Q_2^t Q_1} \text{Tr}_{Q_1} V_1 \text{Tr}_{Q_2} V_2$ in this expression. Upon fusing the representations with the same V_i , (e.g., $\text{Tr}_Q V_3 \text{Tr}_{Q_3} V_3 = \sum_{R_3} N_{QQ_3}^{R_3} \text{Tr}_{R_3} V_3$), and absorbing some innocuous signs into the V_i , we transform to the representation basis by extracting the coefficient of $\text{Tr}_{R_i} V_i$ for three arbitrarily chosen representations R_1, R_2, R_3 . Adjusting the framing, this yields (3.24):

$$C_{R_1 R_2 R_3} = q^{\frac{\kappa_{R_2} + \kappa_{R_3}}{2}} \sum_{Q_1, Q_3, Q} N_{QQ_1}^{R_1} N_{QQ_3}^{R_3} \frac{W_{R_2^t Q_1} W_{R_2 Q_3}}{W_{R_2}}. \quad (4.7)$$

Before proceeding, we wish to make an important observation about one arbitrariness in the above derivation. In principle, we could have derived a similar amplitude

³We are here glossing over the orientations of the relevant link components.

⁴The requisite renormalization of the Ooguri-Vafa operators can again be absorbed in the V_i . We have also suppressed the lengths of the cylinders, since they can be absorbed in the complexified Wilson line V_1, V_2, V_3 of the non-dynamical branes.

with some of the probe branes *above* instead of below the plane of the toric diagram. This would change some of the Ooguri-Vafa operators in (4.2) and result in a slightly different final expression. (Most significantly, a sign $(-1)^{\ell(Q)}$.) Of course, one would then have to match these choices when gluing vertices back together. In the usual formalism, this is clearly best accomplished by putting all probe branes below the plane, as is usually done. The context of the real vertex, however, imposes a different constraint on the probe branes, as we shall see below.

4.2 Hořava operators

In the following, we will employ the same strategy we used in the previous subsection, to derive the real topological vertex. Note first that involution 1 of the conifold requires on the gauge theory side the computation of $SO(N)/Sp(N)$ Chern-Simons amplitudes on S^3 , or $SU(N)$ amplitudes on \mathbb{RP}^3 , depending on whether we choose to deform with μ positive or negative, cmp. subsection 2.2. The SO/Sp picture was used extensively in [4], and we have little reason to reconsider it here. The $SU(N)$ on \mathbb{RP}^3 picture has not so far been developed. But note that since the topological amplitudes do not depend on the deformation parameter, $SU(N)$ on \mathbb{RP}^3 will give exactly the same answer as $SO/Sp(N)$ on S^3 . In particular, the discrete Wilson line around the non-trivial one-cycle of \mathbb{RP}^3 is identified with the distinction between orthogonal and symplectic gauge group.

For involutions 2 and 3, we require the computation of Chern-Simons amplitudes on the three-orbifold S^3/\mathbb{Z}_2 , where the \mathbb{Z}_2 acts with an S^1 fixed locus.⁵ Chern-Simons theory in the presence of precisely such \mathbb{Z}_2 orbifold singularities was studied a good while ago by Hořava [8]. The main result of [8] that we can use is the equivalence of Chern-Simons theory on orbifolds with Chern-Simons theory on smooth manifolds with additional Wilson line insertions. Let's recall the basic idea.

In general, of course, field theories on orbifolds are ill defined because of the violation of unitarity at the orbifold singularities. As argued in [8], however, the absence of local excitations eliminates this difficulty in topological field theories such as Chern-Simons theory. In fact, this must be so because Chern-Simons theory is equivalent to an open string theory [14], and we know that string theory on orbifolds is perfectly well defined.

For Chern-Simons theory, the most interesting orbifold singularities are those in codimension 2. Topologically, we can construct a smooth three-manifold X by cutting

⁵If $S^3 \cong \{\sum x_i^2 = 1\} \subset \mathbb{R}^4$, the relevant involution is $(x_1, x_2, x_3, x_4) \rightarrow (x_1, x_2, -x_3, -x_4)$.

out a tubular neighborhood of the singular locus of the orbifold and replacing it with a collection of solid tori. (Locally, a connected component of the tubular neighborhood is $S^1 \times D/\Gamma$, where Γ is a discrete group acting on the unit disk D , fixing the origin. This can be smoothed in an obvious way.) It was argued in [8] that Chern-Simons theory on such an orbifold O is equivalent to Chern-Simons theory on X , obtained by replacing each component C_α of the singular locus with a collection of Wilson lines,

$$H(C_\alpha) = \sum_R c_{R,\alpha} W_R(C_\alpha), \quad (4.8)$$

where $c_{R,\alpha}$ are some complex coefficients whose calculation is described in [8]. Namely,

$$\langle \Phi \rangle_O = \langle \Phi \prod_\alpha H(C_\alpha) \rangle_X, \quad (4.9)$$

where Φ is any additional observable. There are several subtleties in the formulas (4.8) and (4.9). We mention just a few. For one, the relation between the set of observables on the theory on X to the observables of the orbifold theory is not obvious. This is related to the statement that the gauge group of the theory on X might differ from the gauge group on O by some discrete factor. Moreover, the Wilson lines appearing in the expansion (4.8) need to be appropriately framed. We shall refer to $H(C_\alpha)$ as the Hořava operator.

In the problem of our interest, $O = S^3/\mathbb{Z}_2$ with singular locus S^1 , it is not hard to see that X is again a copy of S^3 (albeit of half the size of the original one). We will not compute the Hořava operator (4.8) from first principles, but instead use the results for the vacuum amplitudes from subsection 3.1.

We begin with involution 3 of the conifold.⁶ Referring back to (3.10), and using that $C_{..R} = W_R = e^{-t\ell(R)/2} \mathcal{W}_R$, $\mathcal{W}_R = \langle \text{Tr}_R U \rangle_{S^3} / \langle \cdot \rangle_{S^3}$, we see that we can write

$$\begin{aligned} Z_{\text{con.}}^3 &= \langle \cdot \rangle_{S^3/\mathbb{Z}_2} \\ &= \frac{1}{S_{00}} \sum_{R=R^t} (-1)^{(\ell(R)-r(R))/2} e^{-t\ell(R)} \langle \text{Tr}_R U \rangle_{S^3}. \end{aligned} \quad (4.10)$$

⁶At first sight, it appears surprising that we would need two different Hořava operators, given that involutions 2 and 3 are related by a flop of the resolved conifold, and indistinguishable on the deformed conifold. A similar puzzle arises, without orientifold, on the conifold with probe branes on the external legs. The toric picture shows that the distinction between the two situation is the channel in which we choose to factorize.

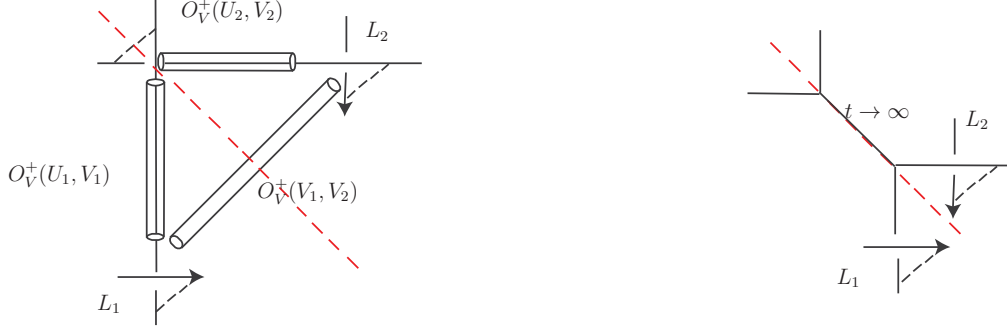


Figure 6: The D-brane configuration relevant for the derivation of the real topological vertex.

From this we deduce that the Hořava operator is given by,

$$H_3 = \frac{1}{S_{00}} \sum_{R=R^t} (-1)^{(\ell(R)-r(R))/2} e^{-t\ell(R)} \text{Tr}_R U, \quad (4.11)$$

with canonically framed Wilson lines $U = P \exp \oint A$ along the fixed S^1 .

For involution 2, we consider (3.16), and identify the factor $q^{-\kappa(R)/4}$ as a fractional framing of the Wilson line. Thus, we can write

$$Z_{\text{con.}}^2 = \frac{1}{S_{00}} \sum_R (-1)^{(\ell(R)-c(R))/2} e^{-t\ell(R)} \langle \text{Tr}_R U_{1/2} \rangle_{S^3}, \quad (4.12)$$

where the subscript indicates the fractional framing of the Wilson line. This gives the Hořava operator

$$H_2 = \frac{1}{S_{00}} \sum_R (-1)^{(\ell(R)-c(R))/2} e^{-t\ell(R)} \text{Tr}_R U_{1/2}. \quad (4.13)$$

4.3 Derivation of the real vertex

With Hořava operators in hand, we now proceed with the derivation of the full real vertex. We consider the D-brane configuration depicted in figure 6.

Note that since any A-type involution acts by complex conjugation, and the direction perpendicular to the r_α - r_β plane of the toric diagram is given by $r_\gamma = \text{Im}(\prod z_i)$ (see (2.1)), probe branes switch the side under the involution. One way to obtain an invariant brane configuration is to insert L_1 above the plane, and L_2 below the plane. The other option will be considered below. Before taking account of the involution, we have the following Ooguri-Vafa operators:

$$O_V^+(U_1, V_1), \quad O_V^+(U_2, V_2), \quad O_V^+(V_1, V_2), \quad (4.14)$$

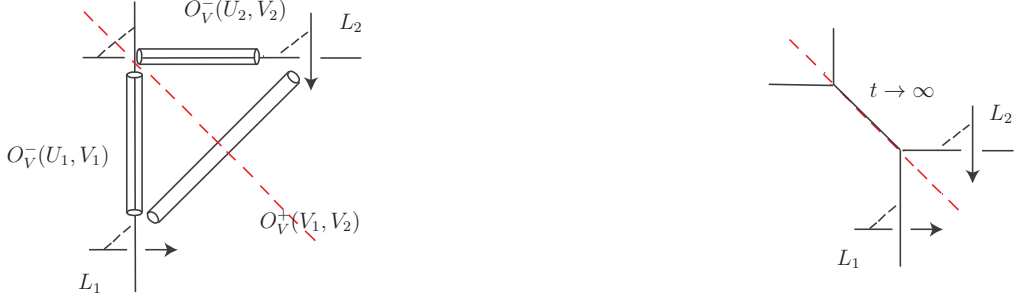


Figure 7: Derivation of the twisted real vertex.

where the third operator accounts for the annulus stretching between L_1 and L_2 .

We now wish to quotient this configuration by the A-type involution exchanging L_1 and L_2 . This first of all leads to the restriction $V_1 = V_2$. Moreover, we have to replace the third Ooguri-Vafa operator above, which came from integrating out the annulus, with the corresponding operator for a Möbius strip. This operator is given by

$$\sum_Q \text{Tr}_Q V_1, \quad (4.15)$$

so we obtain the amplitude

$$Z_{\text{con.}}^3(V_1) = \frac{1}{S_{00}} \sum_{Q, Q_1} \langle \text{Tr}_{Q_1} U_1 \rangle_{S^3/\mathbb{Z}_2} e^{-t\ell(Q_1)} \text{Tr}_{Q_1} V_1 \text{Tr}_Q V_1. \quad (4.16)$$

Applying the rule (4.9) with Hořava operator given by (4.11), this becomes

$$\sum_{\substack{R=R^t \\ Q, Q_1}} \mathcal{W}_{Q_1 R} e^{-t(\ell(R)+\ell(Q_1))} (-1)^{(\ell(R)-r(R))/2} \text{Tr}_{Q_1} V_1 \text{Tr}_Q V_1. \quad (4.17)$$

In the limit $t \rightarrow \infty$, transforming to the representation basis and fusing the representations Q and Q_1 , this gives the real vertex with trivial fixed leg:

$$C_{R_1}^{\text{real}} = q^{\kappa_{R_1}/4} \sum_{QQ_1} N_{QQ_1}^{R_1} W_{Q_1}, \quad (4.18)$$

where the prefactor $q^{\kappa_{R_1}/4}$ adjusts to the canonical framing.

Now let us consider the situation in which L_1 is inserted below the plane, and L_2 above the plane, as depicted in figure 7, This changes the Ooguri-Vafa operators (4.14) into

$$O_V^-(U_1, V_1), \quad O_V^-(U_2, V_2), \quad O_V^+(V_1, V_2). \quad (4.19)$$

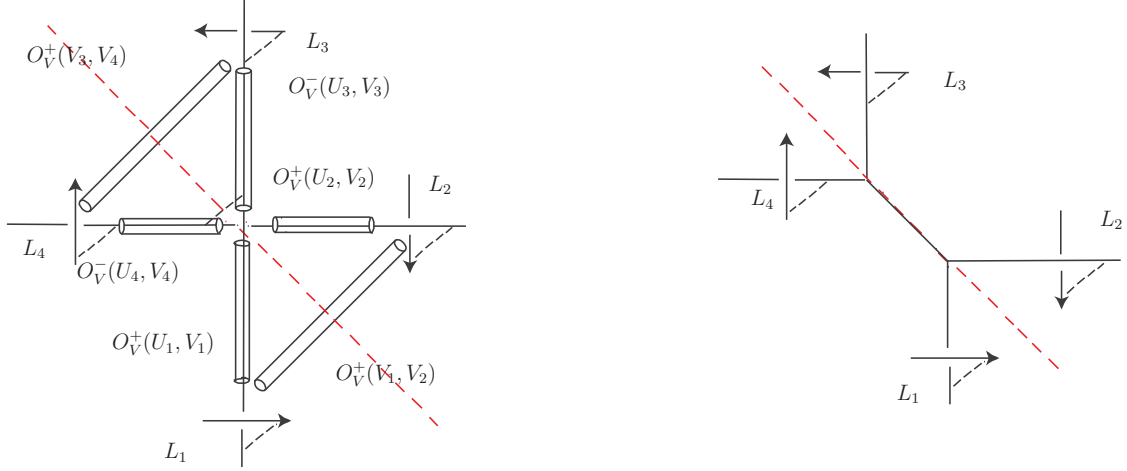


Figure 8: Derivation of the real conifold vertex.

Repeating the same steps as above, we obtain ⁷

$$\tilde{C}_{R_1}^{\text{real}} = q^{\kappa_{R_1}/4} \sum_{QQ_1} (-1)^{\ell(Q)} N_{QQ_1}^{R_1} W_{Q_1}, \quad (4.20)$$

which, because of the extra sign, we named the “twisted” real vertex in equation (3.26).

What about the real vertex with non-trivial representation on the fixed leg? We have not been able to identify a brane configuration that would allow for its direct computation from Chern-Simons theory. However, as we have remarked in subsection 3.2, we never need this amplitude in practice as long as we exclude external branes on fixed legs. Instead, we derive the amplitude (3.27) for the (orientifold of) conifold with branes on all external legs. All amplitudes can be built on that together with the ordinary topological vertex.

The relevant brane configuration is shown in figure 8. Note that we have inserted branes L_1 and L_4 above the plane and L_2 and L_3 below the plane. This is the correct choice compatible with cutting the toric diagram into pieces “from above” on one side of the fixed line, and “from below” on the other side of the fixed line, as required by orientifold invariance.

Applying the by now familiar procedure, we obtain the following expression for this

⁷ We use that $(-1)^{\ell(Q_1)+\ell(R_1)} N_{QQ_1}^{R_1} = (-1)^{\ell(Q)} N_{QQ_1}^{R_1}$.

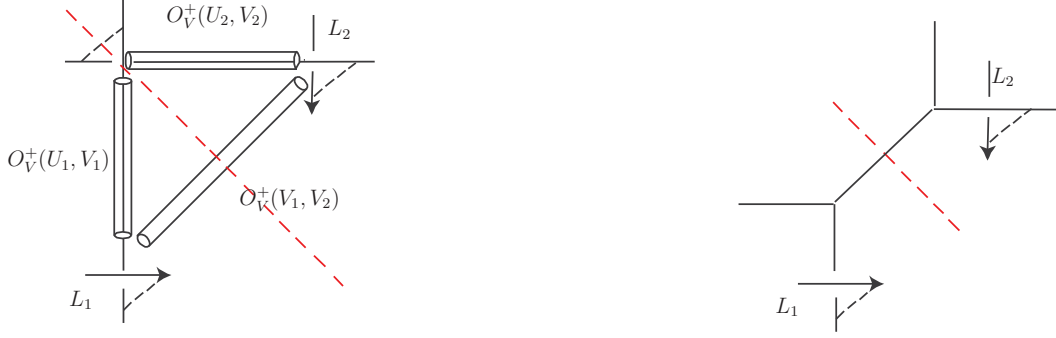


Figure 9: Involution 2 with external branes.

amplitude in the representation basis

$$\begin{aligned}
Z_{\text{con.}}^3(R_1, R_3) &= \\
&= \sum e^{-(\ell(R)+\ell(Q_1)+\ell(Q_3))t} N_{Q_1}^{R_1} N_{\tilde{Q}_3}^{R_3^t} (-1)^{\ell(\tilde{Q})} (-1)^{(\ell(R)-r(R))/2} \langle \text{Tr}_R U \text{Tr}_{Q_3} U_3 \text{Tr}_{Q_1} U_1 \rangle_{S_3} \\
&= \sum e^{-\ell(R)t/2} N_{Q_1}^{R_1} N_{\tilde{Q}_3}^{R_3^t} (-1)^{\ell(R_3)+\ell(\tilde{Q})} (-1)^{(\ell(R)-r(R))/2} \frac{W_{Q_1 R} W_{Q_3 R}}{W_R} \\
&= q^{\frac{\kappa_{R_1} + \kappa_{R_3}}{4}} \sum_{R=R^t} C_{R_1 R}^{\text{real}} (-1)^{(\ell(R)-r(R))/2} e^{-t\ell(R)/2} \tilde{C}_{R_3^t R}^{\text{real}}.
\end{aligned} \tag{4.21}$$

This result is compatible with the real vertex formalism as described in section 3, in particular the sign rules discussed in subsection 3.3.

Finally, we comment on involution 2 with branes on the external legs of the conifold, see figure 9. Using the Hořava operator (4.13), it is straightforward to derive the following amplitude for this configuration

$$Z_{\text{con.}}^2(R_1) = \sum_R W_{R_1 R} e^{-t\ell(R)/2} q^{-\frac{\kappa_R + \kappa_{R_1}}{4}} (-1)^{(\ell(R)-c(R))/2}. \tag{4.22}$$

Again, this is compatible with the formalism of section 3. The main interest of the formula is the factor $q^{-\kappa_{R_1}/4}$, which again comes from the fractional framing of the Wilson loop insertion in Chern-Simons theory.

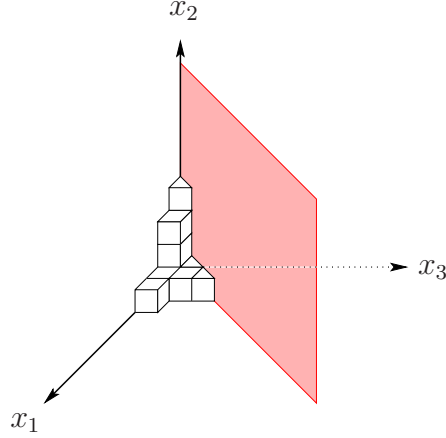


Figure 10: Three-dimensional partition with fixed asymptotics along the three axes, and symmetry plane at $x_1 = x_3$.

5 Melting crystal

Soon after its discovery, the topological vertex was related to a statistical mechanics model of a melting crystal corner [9]. The relation can be expressed in the formula

$$C_{R_1 R_2 R_3}(1/q) = q^{\frac{\|R_1^t\|^2 + \|R_2^t\|^2 + \|R_3^t\|^2}{2}} P_{R_1 R_2 R_3}(q) M(q)^{-1}, \quad (5.1)$$

where $C_{R_1 R_2 R_3}$ is the topological vertex, which in the context of the melting crystal is conveniently written in terms of skew Schur functions

$$C_{R_1 R_2 R_3}(q) = q^{\frac{\kappa_{R_3} + \kappa_{R_2}}{2}} s_{R_2^t}(q^\rho) \sum_Q s_{R_1/Q}(q^{\rho+R_2^t}) s_{R_3^t/Q}(q^{\rho+R_2}). \quad (5.2)$$

On the right hand side of (5.1), $P_{R_1 R_2 R_3}$ is the generating function counting three-dimensional partitions with fixed asymptotics along the three axes given by the two-dimensional partitions R_1, R_2, R_3 . The q -weight of each box in the 3d partition is 1 minus the number of 2d partitions containing that box. See figure 10. Furthermore, $M(q) = \prod_{n=1}^{\infty} (1 - q^n)^{-n}$ is the MacMahon function counting 3d partitions with trivial asymptotics, and the prefactor containing

$$\|R_i\|^2 = \sum_i \lambda_i^2, \quad (5.3)$$

accounts for the adjustment of the framing and the gluing algorithm.

In this section, we explain the interpretation of the real topological vertex, which we have developed in this paper, in the melting crystal picture. We will find that both straight and twisted real vertex admit a melting crystal interpretation.

5.1 Melting crystal interpretation of the real vertex

The positive axes of figure 10 can be essentially identified with the toric diagram of \mathbb{C}^3 . Referring back to the action of the anti-holomorphic involution on this toric diagram (see figure 1 on page 6), it is then clear what we have to do: We should count 3d partitions, with fixed asymptotics, which are invariant under the symmetry exchanging two of the axes. The 2d partitions constraining the asymptotics must then satisfy the constraint $R_3 = R_1^t$, $R_2 = R_2^t$.

To prepare for the answer to expect, we record here the partition function of symmetric plane partitions with empty asymptotics. This partition function was originally conjectured by MacMahon [15]; a proof was given by Macdonald [12] and Andrews [16], The formula is

$$M^{\text{sym}}(q) = \prod_{n=1}^{\infty} (1 - q^{2n-1})^{-1} \prod_{n=1}^{\infty} (1 - q^{2n})^{-[n/2]}. \quad (5.4)$$

In this formula, symmetric partitions are weighted by the *total* number of boxes. From the orientifold point of view, it is more natural to count only the boxes on one side of the symmetry plane. This can be implemented by the transformation $q \rightarrow q^{1/2}$ in (5.4), and we define the real MacMahon function by

$$M^{\text{real}}(q) = M^{\text{sym}}(q^{1/2}). \quad (5.5)$$

Now let us study this in more detail. Following [9], we confine our symmetric 3d partitions into a box of finite size N^3 , with boundary condition in the (x_2, x_3) -plane at $x_1 = N$ given by the 2d partition R . We assume trivial boundary condition in the x_2 direction.

We want to use the transfer matrix approach of [9], so we should slice the partition diagonally. This yields a stack of partitions $\nu(t)$, indexed by the coordinate t of the corresponding slice. The $\nu(t)$ satisfy the interlacing condition

$$R = \nu(-N) \prec \nu(-N + 1) \prec \cdots \prec \nu(-1) \prec \nu(0), \quad (5.6)$$

where two partitions μ and ν are said to interlace, $\mu \prec \nu$, if

$$\mu_l \leq \nu_l \leq \cdots \leq \mu_2 \leq \nu_2 \leq \mu_1 \leq \nu_1, \quad (5.7)$$

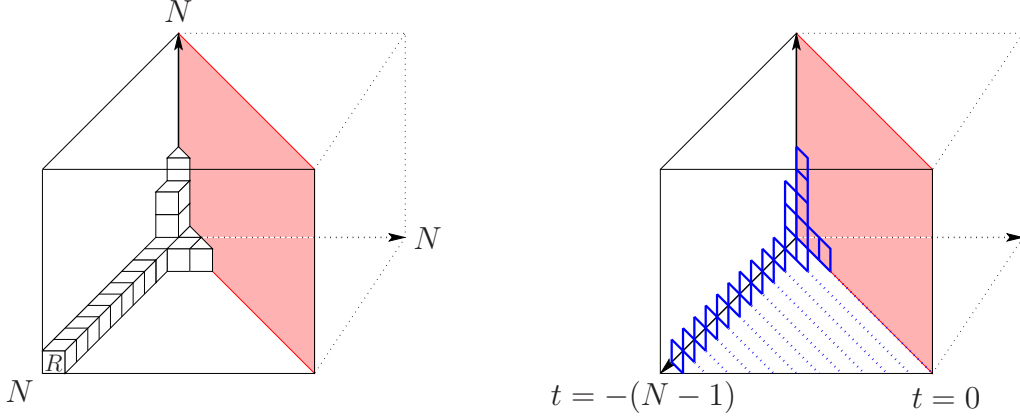


Figure 11: Left: (Half of) a symmetrically melting crystal in a finite box of volume N^3 with fixed boundary condition given by a 2d partition R . Right: Diagonal slicing of the setup.

holds, with μ_i and ν_i the i -th part of the partition, and l is the number of parts. In distinction to arbitrary 3d partitions, the condition (5.6) is not followed by a similar condition at $t > 0$. Rather, the partitions at $t > 0$ are determined by those at $-t$, and the partition at $t = 0$ is essentially arbitrary.

We continue to follow [9]. To each partition μ , we associate the state $|\mu\rangle$ in the Hilbert space of a complex fermion. Moreover, we introduce, via bosonization, the operator $\Gamma_-(z)$ with the property

$$\Gamma_-(1)|\mu\rangle = \sum_{\nu \succ \mu} |\nu\rangle, \quad (5.8)$$

where $\nu \succ \mu$ is equivalent to $\mu \prec \nu$.

It is then clear that we can obtain the partition function $P_R^{(N)}$ of the symmetric crystal in the cubic box of volume N^3 with fixed boundary R at $x = N$ (or $t = -N$ in diagonal coordinates) via successive application of $\Gamma_-(1)$ operators on the state $|R\rangle$ and summing over all possible partitions λ at $t = 0$,

$$P_R^{(N)}(q) = q^{-\binom{R}{2}} \sum_{\lambda} \left\langle \lambda \left| q^{L_0/2} \prod_{t=-N+1}^{-1} \Gamma_-(1) q^{L_0} \right| R \right\rangle, \quad (5.9)$$

where the factor of $q^{-\binom{R}{2}}$ with $\binom{R}{2} := \sum_i \binom{R_i}{2}$ accounts for the increase of boxes due to the diagonal slicing [9]. The extra factor $q^{L_0/2}$ counts half the number of boxes at $t = 0$.

Using the commutation relation $\Gamma_-(z) = z^{-L_0}\Gamma_-(1)z^{L_0}$, we obtain

$$P_{R\cdot}^{(N)}(q) = q^{-\binom{R}{2} + (N-1/2)\ell(R)} \sum_{\lambda} \left\langle \lambda \left| \prod_{i=0}^{N-2} \Gamma_-(q^{-1/2-i}) \right| R \right\rangle. \quad (5.10)$$

Applying the fundamental identity (see for instance [17])

$$\prod_i \Gamma_-(x_i) |\lambda\rangle = \sum_{\mu} s_{\mu/\lambda}(x^{-1}) |\mu\rangle, \quad (5.11)$$

we infer

$$P_{R\cdot}^{(N)}(q) = q^{-\binom{R}{2} + (N-1/2)\ell(R)} \sum_{\mu} s_{\mu/R}(q^{-\rho}), \quad (5.12)$$

with $q^{\rho} := (q^{-1/2}, q^{-3/2}, \dots)$. Finally, invoking the Schur function identity (see for instance [12])

$$\sum_{\mu} s_{\mu/\lambda}(x) = \prod_i \frac{1}{1-x_i} \prod_{i<j} \frac{1}{1-x_i x_j} \sum_{\nu} s_{\lambda/\nu}(x), \quad (5.13)$$

we obtain

$$P_{R\cdot}^{(N)}(q) = M_N^{\text{real}}(q) q^{-\binom{R}{2} + (N-1/2)\ell(R)} \sum_{\lambda} s_{R/\lambda}(q^{-\rho}), \quad (5.14)$$

where we have written the prefactor as

$$M_N^{\text{real}}(q) = \prod_{i=1}^{N-1} \frac{1}{1-q^{-\rho_i}} \prod_{1 \leq i < j}^{N-1} \frac{1}{1-q^{-\rho_i - \rho_j}} = \prod_{n=1}^{N-1} \frac{1}{1-q^{n-1/2}} \prod_{n=1}^{N-1} \frac{1}{(1-q^n)^{\lfloor n/2 \rfloor}}. \quad (5.15)$$

In the limit $N \rightarrow \infty$, we recover the real MacMahon function (5.5) as the partition function of the symmetrically melting crystal (up to $q \rightarrow q^{1/2}$) with empty boundary condition, $R = \cdot$.

For non-trivial representation R , we use the relation

$$\frac{\|R\|^2}{2} := \sum_i \frac{R_i^2}{2} = \binom{R}{2} + \ell(R), \quad (5.16)$$

to deduce (the rescaling in the limit is discussed and interpreted in detail in [9])

$$P_{R\cdot}(q) := \lim_{N \rightarrow \infty} q^{-N\ell(R)} P_{R\cdot}^{(N)}(q) = M^{\text{real}}(q) q^{-\frac{\|R\|^2}{2}} \sum_{\lambda} s_{R/\lambda}(q^{-\rho}). \quad (5.17)$$

This expression should be compared with the expression (3.29) for the real topological vertex in terms of Schur functions. In the one-leg case, this simplifies to

$$C_{R\cdot}^{\text{real}}(q) = q^{\frac{\|R\|^2 - \|R^t\|^2}{4}} \sum_{\lambda} s_{R^t/\lambda}(q^{\rho}), \quad (5.18)$$

where we used the relation $\kappa_R = \|R\|^2 - \|R^t\|^2$.

The relation between (5.17) and (5.18) is explicitly

$$C_{R^\cdot}^{\text{real}}(1/q) = q^{\frac{\|R\|^2 + \|R^t\|^2}{4}} P_{R^t^\cdot}(q) M^{\text{real}}(q)^{-1}. \quad (5.19)$$

Including the framing factors, this relation between the real vertex and symmetric crystal melting fits beautifully into the usual relation between topological vertex and crystal melting expressed in (5.1). (The seeming replacement of R with R^t on the right hand side has to do with our choice of labelling the melting crystal representation with the asymptotics along the x_1 -axis, $R = R_1$. A choice that matches better the clockwise conventions of subsection 3.3 is to use $R_3 = R_1^t = R^t$.)

To give a similar interpretation of the twisted real vertex (3.26), we weight each representation in (5.9) by an additional minus sign $(-1)^{\ell(\lambda)}$. In other words, we replace $q^{L_0/2}$ with $(-q)^{L_0/2}$. Repeating the steps above, we obtain

$$\tilde{P}_{R^\cdot}(q) = (-1)^{\ell(R)} M^{\text{real}}(1/q) q^{-\frac{\|R\|^2}{2}} \sum_{\lambda} s_{R^t/\lambda}(q^\rho). \quad (5.20)$$

This has to be compared with the twisted real topological vertex (3.30)

$$\tilde{C}_{R^\cdot}^{\text{real}}(q) = (-1)^{\ell(R)} q^{\frac{\|R\|^2 - \|R^t\|^2}{4}} \sum_{\lambda} s_{R/\lambda}(q^{-\rho}). \quad (5.21)$$

We deduce that

$$\tilde{C}_{R^\cdot}^{\text{real}}(1/q) = q^{\frac{\|R\|^2 + \|R^t\|^2}{4}} \tilde{P}_{R^t^\cdot}(q) M^{\text{real}}(1/q)^{-1}. \quad (5.22)$$

Again, this fits with (5.1). Note that the only difference with (5.19) lies in the slightly different normalization by the real MacMahon function (5.5).

5.2 Constant map contribution in orientifolds

It was observed in [11] that the constant map contribution to the free energy of the topological string on the Calabi-Yau manifold X is encoded in the asymptotic expansion of the MacMahon function. Namely, it is known that the constant maps of genus g Riemann surface into X contribute [21]

$$\frac{\chi}{2} n_0^g = \frac{\chi}{2} \int_{\mathcal{M}_g} c_{g-1}^3(\mathcal{E}), \quad (5.23)$$

where χ is Euler characteristic of X , \mathcal{M}_g is the moduli space of Riemann surfaces, \mathcal{E} is the Hodge bundle over \mathcal{M}_g , and c_{g-1} is its $(g-1)$ -st Chern class. This Hodge integral

is well-known [18], and one obtains

$$n_0^g = \frac{|B_{2g}B_{2g-2}|}{2g(2g-2)(2g-2)!}, \quad (5.24)$$

where B_{2g} are the Bernoulli numbers. These are precisely the coefficients of the asymptotic expansion of the MacMahon function at $g_s = -\log q \rightarrow 0$ (see appendix E of [19]):

$$\begin{aligned} \log M(q) \equiv \mathcal{F}^{\text{even}}(g_s) &= \sum_n \frac{q^n}{n(1-q^n)^2} \\ &\sim \frac{1}{g_s^2} \zeta(3) - \frac{1}{12} \log g_s + \sum_{g \geq 2} g_s^{2g-2} n_0^g + \text{const.} \end{aligned} \quad (5.25)$$

The first two terms can be interpreted as the $g = 0$ and $g = 1$ contribution, respectively. The constant has no obvious interpretation. Moreover given the factorial growth of the coefficients $n_0^g \sim (2g-1)(2g-3)!$, the above expansion has zero convergence radius and there can be non-perturbative corrections which can be worked out by means of the Borel analysis. After writing the coefficients as:

$$n_0^g = \frac{B_{2g}}{2g(2g-2)!(2g-2)} \left(2(2g-2)! \sum_{m=1} \frac{1}{(2\pi im)^{2g-2}} \right), \quad (5.26)$$

we define the Borel transform by dividing each coefficient by its factorially divergent part to construct a series with finite convergence radius:

$$\begin{aligned} B[\mathcal{F}^{\text{even}}](\xi) &= \sum_{g=2}^{+\infty} \frac{n_0^g}{(2g-3)!} \xi^{2g-2} = \sum_{g=2}^{+\infty} \frac{B_{2g}}{2g(2g-2)!} \sum_{m \in \mathbb{Z}} \frac{\xi^{2g-2}}{(2\pi im)^{2g-2}} \\ &= \sum_{m \in \mathbb{Z}} \left(-\frac{1}{12} + \frac{(2\pi im)^2}{\xi^2} - \frac{1}{4} \frac{1}{\sinh^2\left(\frac{\xi}{4\pi im}\right)} \right). \end{aligned} \quad (5.27)$$

The inverse of this transform is given by:

$$\tilde{\mathcal{F}}^{\text{even}}(g_s) = \frac{1}{4} \sum_{m \in \mathbb{Z}} \int_0^{+\infty} \frac{ds}{s} \left(\frac{1}{\sin^2\left(\frac{g_s}{4\pi m} s\right)} - \left(\frac{4\pi m}{g_s}\right)^2 \frac{1}{s^2} - \frac{1}{3} \right) e^{-s}. \quad (5.28)$$

Notice that for a convergent series $F(x)$ with sum $f(x)$, the inverse Borel transform $\tilde{F}(x)$ is such that $\tilde{F}(x) = f(x)$. In the asymptotic case, the inverse Borel transform can be used, when the integral is well defined, to assign a value to the divergent sum. However, when the integral of the inverse transform is ill defined—which is the case for non Borel-summable series—one needs to modify the integration contour. This

procedure is a priori not unique and it affects the reconstruction of the original series by introducing the so called non-perturbative ambiguity. Indeed the integral (5.28) is ill defined since there are poles on the real axis. However, in the present case, there is a natural prescription to deform the contour and compute un-ambiguously the full non-perturbative correction since the inverse Borel transform (5.28) coincides, up to a trivial change of variables, with the integral representation proposed by Gopakumar-Vafa for the constant map [11]. The Gopakumar-Vafa integral formula has in turn a Schwinger-like interpretation as the four-dimensional one-loop effective action obtained by integrating out $D0$ -branes degrees of freedom in a constant self-dual gravi-photon field-strength. From this viewpoint, it is clear that the imaginary part of the integral (5.28) gives the absorptive part of the action that is the non-perturbative production rate of $D0$ -branes bound states. The imaginary part of the integral can be computed with the $+i\epsilon$ prescription (rotating the contour by $+\pi/2$) and closing the contour to pick all the residues, the result reads

$$\begin{aligned} \text{Im } \tilde{\mathcal{F}}^{\text{even}}(g_s) &= \frac{\pi}{4} \sum_{n=1}^{+\infty} \sum_{m \in \mathbb{Z}} \oint_{n\pi} \frac{d\sigma}{2\pi i} \frac{1}{\sigma} \left(\frac{1}{\sin^2 \sigma} - \frac{1}{\sigma^2} - \frac{1}{3} \right) e^{-\frac{4\pi m}{g_s} \sigma} \\ &= -\frac{1}{4\pi g_s} \sum_{n,m=1}^{+\infty} \left(\frac{4\pi^2 m}{n} + \frac{g_s}{n^2} \right) e^{-\frac{4\pi^2 mn}{g_s}}. \end{aligned} \quad (5.29)$$

This provides the full non-perturbative contribution to the McMahon function.⁸ The instanton action $A = 4\pi^2 m$ governs the production rate of bounds states of mass $2\pi m$, the integer m counts the winding along the M-theory circle [11], while the integer n is the instanton number.

In the previous subsection, we have seen that in the context of the real topological vertex, the MacMahon function is replaced with its real version, $M^{\text{real}}(q)$. It is natural to expect that this relation is more general, and that the real MacMahon function will capture the constant map contribution to the real topological string on a general Calabi-Yau manifold.⁹ More precisely, we propose that in the large volume limit on a Calabi-Yau X , the real topological string partition function behaves as

$$\mathcal{G} \sim_{t \rightarrow \infty} \frac{\chi_a}{2} \log M^{\text{real}}(q) + \frac{\chi_b}{2} \log M(q), \quad (5.30)$$

⁸See [20] for more details.

⁹Note that at this time of writing, we are not aware of a published physical derivation, nor a mathematical theory, of this contribution. A rough estimate based along the lines of [21] is consistent with our present results—the perturbative contributions vanish for positive worldsheet Euler characteristic.

with $\chi_a + 2\chi_b = \chi$ and χ as in (5.23). To explore the consequences of this conjecture, let us expand $M^{\text{real}}(q)$ around $g_s = 0$. First we write

$$\begin{aligned} \log M^{\text{real}}(q) &= \sum_n \frac{q^n}{2n(1-q^n)^2} + \sum_{n \text{ odd}} \frac{q^{n/2}}{n(1-q^n)} \\ &= \frac{1}{2} \log M(q) + \mathcal{F}^{\text{odd}}(g_s), \end{aligned} \quad (5.31)$$

which is the natural split in even and odd under $g_s \rightarrow -g_s$ ($q \rightarrow q^{-1}$). The even part is 1/2 times the closed string result (5.25), which is the expected result from the point of view of the real topological string. For the odd part, we use the expansion

$$\frac{1}{2 \sinh \frac{x}{2}} = \frac{1}{x} + \sum_{k=1}^{\infty} (-1)^k \frac{2x}{x^2 + (2\pi k)^2}, \quad (5.32)$$

to obtain

$$\begin{aligned} \sum_{n=1}^{\infty} \frac{q^{n/2}}{n(1-q^n)} &= \sum_{n=1}^{\infty} \frac{1}{n} \left(\frac{1}{ng_s} + \sum_{k=1}^{\infty} (-1)^k \frac{2ng_s}{(ng_s)^2 + (2\pi k)^2} \right) \\ &= \frac{1}{g_s} \zeta(2) + \sum_{k=1}^{\infty} \frac{(-1)^k}{k} \left(-\frac{g_s}{4\pi^2 k} + \frac{1}{2} \coth \frac{2\pi^2 k}{g_s} \right) \\ &= \frac{1}{g_s} \zeta(2) - \frac{1}{2} \log 2 + \frac{g_s}{16\pi^2} \zeta(2) + \sum_{k,n=1}^{\infty} \frac{(-1)^k}{k} e^{-4\pi^2 kn/g_s}. \end{aligned} \quad (5.33)$$

Putting things together, this yields:

$$\mathcal{F}^{\text{odd}}(g_s) = \frac{3\zeta(2)}{4g_s} - \frac{1}{4} \log 2 + \sum_{k,n=1}^{\infty} \frac{(-1)^k}{k} \left(e^{-4\pi^2 kn/g_s} - \frac{1}{2} e^{-2\pi^2 kn/g_s} \right). \quad (5.34)$$

We emphasize that this is a convergent expansion, with perturbative contributions vanishing beyond one-loop. Quite interestingly, the constant appears to be violating the behaviour under $g_s \rightarrow -g_s$ that we imposed on $\mathcal{F}^{\text{odd}}(g_s)$. One may check that this is corrected by the non-perturbative contributions.

To see this, we introduce the variable $p = \exp(-\frac{4\pi^2}{g_s})$ and perform the sum over n in (5.34) to write:

$$\mathcal{F}^{\text{odd}}(g_s) = \frac{3\zeta(2)}{4g_s} - \frac{1}{4} \log 2 + \sum_{k=1}^{\infty} \frac{(-1)^k}{k} \left(\frac{p^k}{1-p^k} - \frac{1}{2} \frac{p^{k/2}}{1-p^{k/2}} \right). \quad (5.35)$$

Under $g_s \rightarrow -g_s$ we have

$$\frac{p}{1-p} \rightarrow -\frac{1}{1-p} = -\frac{p}{1-p} - 1, \quad (5.36)$$

from which follows ¹⁰

$$\begin{aligned}\mathcal{F}^{\text{odd}}(-g_s) &= -\frac{3\zeta(2)}{4g_s} - \frac{1}{4}\log 2 - \sum_{k=1}^{\infty} \frac{(-1)^k}{k} \left(\frac{p^k}{1-p^k} - \frac{1}{2} \frac{p^{k/2}}{1-p^{k/2}} + \frac{1}{2} \right) \\ &= -\frac{3\zeta(2)}{4g_s} + \frac{1}{4}\log 2 - \sum_{k=1}^{\infty} \frac{(-1)^k}{k} \left(\frac{p^k}{1-p^k} - \frac{1}{2} \frac{p^{k/2}}{1-p^{k/2}} \right) = -\mathcal{F}^{\text{odd}}(g_s).\end{aligned}\tag{5.37}$$

So in the case of the real McMahon function it is essential to include the non-perturbative contribution to obtain a definite-parity asymptotic expansion.

Finally, we shall give a Schwinger-like interpretation to the non-perturbative terms in $\mathcal{F}^{\text{odd}}(g_s)$ similar to that for the even part. To this end, we rewrite $\mathcal{F}^{\text{odd}}(g_s)$ in terms of the integral representation

$$\mathcal{F}^{\text{odd}}(g_s) = \sum_{n=-\infty}^{\infty} (-1)^n \int_{\epsilon}^{\infty} \frac{ds}{s} \frac{e^{-2\pi is(n/2)}}{2 \sinh(g_s s/2)},\tag{5.38}$$

which furthermore can be split into

$$\mathcal{F}^{\text{odd}}(g_s) = \sum_{n=-\infty}^{\infty} \int_{\epsilon}^{\infty} \frac{ds}{s} \frac{e^{-2\pi is n}}{2 \sinh(g_s s/2)} - \sum_{n \text{ odd}} \int_{\epsilon}^{\infty} \frac{ds}{s} \frac{e^{-2\pi is(n/2)}}{2 \sinh(g_s s/2)}.\tag{5.39}$$

This expression is the result of a two-dimensional Schwinger computation of integrating out a scalar field coupled to a constant $U(1)$ field-strength, where the scalar field has either integral or fractional (half-integer) charge. In order to see that one can indeed derive $\mathcal{F}^{\text{odd}}(g_s)$ from such a computation, note first that under the orientifold projection only the two components of the gravi-photon field $A^\mu(x)$ away from the $O4$ -plane survive, since $A^\mu(x)$ needs to be odd under the projection. Secondly, the occurrence of states with fractional charge, or better momenta, can be inferred from the expectation that one can lift every IIA orientifold to M-theory on a G_2 manifold with some \mathbb{Z}_2 action on the M-theory circle (in our case with fixed-points). The non-trivial action on the M-theory circle results in fractional momentum states. Thus, the Schwinger interpretation of $\mathcal{F}^{\text{odd}}(g_s)$ is in terms of (fractional) bound states of $D0$ -branes living away from the orientifold plane such that they feel the $\mathcal{N} = 2$ of the bulk.

With the Schwinger representation for $\mathcal{F}^{\text{odd}}(g_s)$ at hand one can interpret the non-perturbative contribution in (5.34) as we did for the McMahon function. We evaluate the absorptive part of the integral (5.39) with the $+i\epsilon$ prescription by closing the

¹⁰Recall that $\sum_{k=1}^{\infty} \frac{(-1)^k}{k} = -\log(2)$.

contour to pick the residues at the simple poles and obtain

$$\sum_{k=1} \frac{(-1)^k}{k} \left(\sum_n e^{-\frac{4\pi^2 nk}{g_s}} - \sum_{n \text{ odd}} e^{-\frac{2\pi^2 nk}{\lambda}} \right) = \sum_{k=1} \frac{(-1)^k}{k} \left(2 \sum_n e^{-\frac{4\pi^2 nk}{g_s}} - \sum_n e^{-\frac{2\pi^2 nk}{\lambda}} \right), \quad (5.40)$$

which reproduces indeed the non-perturbative terms in the real McMahon function in (5.34). Notice that this time we have two families of non-perturbative contributions with instanton actions $4\pi^2 n$ and $2\pi^2 n$, which can be interpreted as controlling the production rates of bound states, respectively fractional bound states, of $D0$ -branes.

6 Examples

We now want to illustrate the real topological vertex formalism with its sign subtleties explained in section 3 at hand of a couple of instructive examples. We will check that we obtain a consistent enumerative interpretation in terms of real Gopakumar-Vafa invariants, as well as compatibility of the partition function under flop transitions, and reduction to known invariants at certain points in parameter space.

To write the expansion of the reduced free energy (3.4), we denote the subset of Kähler parameters that are mapped to themselves by the involution σ defining the orientifold of X by Q_A , and those that are identified pairwise by Q'_B . (This is an invariant distinction if we use an integral basis of the second cohomology of X .) The point is that the former set appears with half-integer exponents in $\mathcal{G}'_X{}^\sigma$, and the latter only with integer exponents. The real Gopakumar-Vafa invariants are denoted by ${}^X N_{d_Q, d_{Q'}}^{(\chi)}$, with integer vectors $d_Q, d_{Q'}$ labelling the degree and $\chi \geq -1$ being related to the 5-dimensional spin in the M-theory interpretation as counting of BPS states (see [22]). (If the BPS state is represented by a smooth real curve, χ is the negative of its Euler characteristic.) The expansion is

$$\mathcal{G}'_X{}^\sigma = \sum_{\substack{\chi, d_Q, d_{Q'} \geq 0 \\ k \text{ odd}}} {}^X N_{d_Q, d_{Q'}}^{(\chi)} \frac{1}{k} \left(2i \sin \frac{k g_s}{2} \right)^\chi \prod_A Q_A^{k d_{Q_A}/2} \prod_B Q'_B{}^{k d_{Q'_B}}. \quad (6.1)$$

A typical, though not universal, feature of this expansion is a certain correlation between χ and the degrees d_{Q_A} . Namely, ${}^X N_{d_Q, d_{Q'}}^{(\chi)}$ vanish unless $\chi \equiv \sum_A d_{Q_A} \pmod{2}$. This rule can be explained from the point of view of Gromov-Witten theory along the lines of the arguments in [2] by the local cancellation between boundaries and crosscaps on fixed \mathbb{P}^1 's covered by even degree maps. However, exceptions to this d_Q - χ -correlation

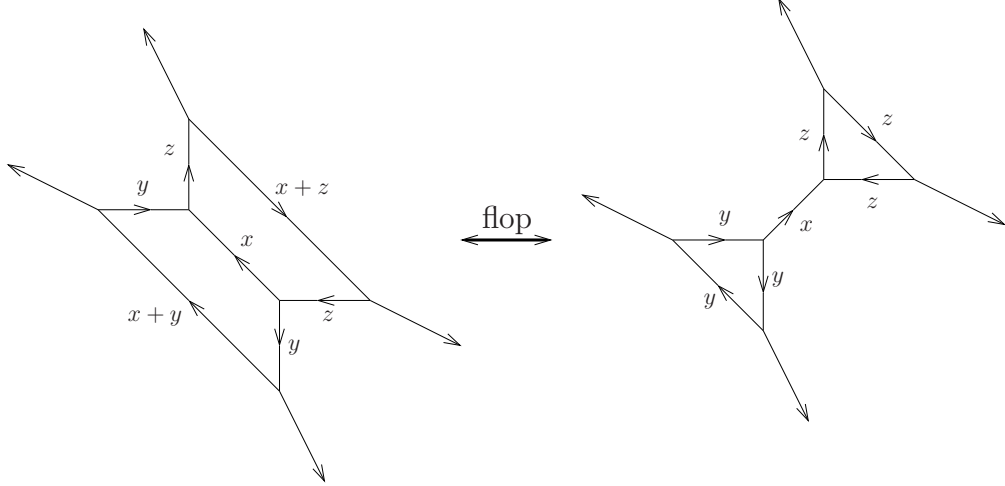


Figure 12: The (p, q) -webs of the butterfly (left) and $[\mathbb{P}^2]^2$ (right) geometry with Kähler moduli associated to the edges. The two geometries are related via a flop of the central \mathbb{P}^1 .

rule are possible when there are even degree maps passing through fixed vertices. A rule that always holds is that ${}^X N_{d_Q, d_{Q'}}^{(\chi)}$ is bounded above by, and equal modulo 2 to, the corresponding complex invariant ${}^X n_{d_Q, d_{Q'}, d_{Q'}}^{(g=\chi+1)}$.

6.1 Butterfly

Consider the two geometries shown in terms of (p, q) -webs in figure 12. We will refer to the left geometry as butterfly, and to the right one as $[\mathbb{P}^2]^2$, since it consists of two local \mathbb{P}^2 's connected via a \mathbb{P}^1 with $\mathcal{O}(-1) \oplus \mathcal{O}(-1)$ normal bundle (conifold). The geometries are related via a flop transition of the central \mathbb{P}^1 . These geometries have been used to study local mirror symmetry (at tree-level) in [23]. We will also refer to the butterfly as phase A and to $[\mathbb{P}^2]^2$ as phase B .

Closed string

An expression for the partition function Z_A of the (closed) topological string on the butterfly can be obtained in terms of the topological vertex (*cf.* [1]) and reads (for the association of representations R_i to edges see figure 13)

$$\begin{aligned}
 Z_A = \sum_R & (-1)^{\ell(R_0) - \ell(R_3) - \ell(R_6)} q^{\sum_{i \neq 0} \kappa_{R_i} / 2} x^{d(x)} y^{d(y)} z^{d(z)} \\
 & \times C_{R_2^t R_4 R_0^t} C_{R_2 R_3^t} C_{R_3 R_1^t} C_{R_5^t R_1 R_0} C_{R_5 R_6^t} C_{R_6 R_4^t},
 \end{aligned} \tag{6.2}$$

where $R = \{R_0, \dots, R_6\}$,

$$\begin{aligned} d(x) &= \ell(R_0) + \ell(R_3) + \ell(R_6), \\ d(y) &= \ell(R_1) + \ell(R_2) + \ell(R_3), \\ d(z) &= \ell(R_4) + \ell(R_5) + \ell(R_6), \end{aligned} \tag{6.3}$$

$x = e^{-t_0}$, $y = e^{-t_1}$ and $z = e^{-t_2}$, where t_i are the three Kähler moduli of the geometry.

Similarly, the partition function Z_B of $[\mathbb{P}^2]^2$ (cf. [4]) is given by

$$\begin{aligned} Z_B &= \sum_R (-1)^{d(x)-d(y)-d(z)} q^{\sum_{i \neq 0} \kappa_{R_i}} x^{d(x)} y^{d(y)} z^{d(z)} \\ &\quad \times C_{R_1 R_2^t R_0} C_{R_3 R_1^t} C_{R_2 R_3^t} C_{R_4 R_5^t R_0} C_{R_6 R_4^t} C_{R_5 R_6^t}, \end{aligned} \tag{6.4}$$

with

$$\begin{aligned} d(x) &= \ell(R_0), \\ d(y) &= \ell(R_1) + \ell(R_2) + \ell(R_3), \\ d(z) &= \ell(R_4) + \ell(R_5) + \ell(R_6). \end{aligned} \tag{6.5}$$

In [23] it was observed that the tree-level instanton pieces of the topological amplitudes of the two phases, expressed in terms of Gopakumar-Vafa invariants $^{A/B}n_{d_x, d_y, d_z}^{(g)}$, are related via ¹¹

$$^A n_{d_x, d_y, d_z}^{(0)} = ^B n_{d_y + d_z - d_x, d_y, d_z}^{(0)}. \tag{6.6}$$

As it must be, and shown rigorously in [24], this relation persists to all genera.

The (p, q) -webs possess three different \mathbb{Z}_2 symmetries, as shown in figure 13. Following the formalism outlined in section 3 we can write down partition functions capturing the respective orientifolds of the theory.

Involution 1

The point-reflection involution acting on the butterfly identifies the Kähler moduli $y = z$ and the orientifold partition function is given by

$$\begin{aligned} Z_A^1 &= \sum_{R, R_0=R_0^t} (-1)^{(\ell(R_0) \pm r(R_0))/2 - \ell(R_3)} q^{\kappa_{R_1}/2 + \kappa_{R_3}/2 + \kappa_{R_5}/2} x^{d(x)} y^{d(y)} \\ &\quad \times C_{R_5^t R_1 R_0} C_{R_5 R_3^t} C_{R_3 R_1^t}, \end{aligned} \tag{6.7}$$

¹¹Except for $^A n_{1,0,0}^{(0)}$, which counts just the flopped \mathbb{P}^1 .

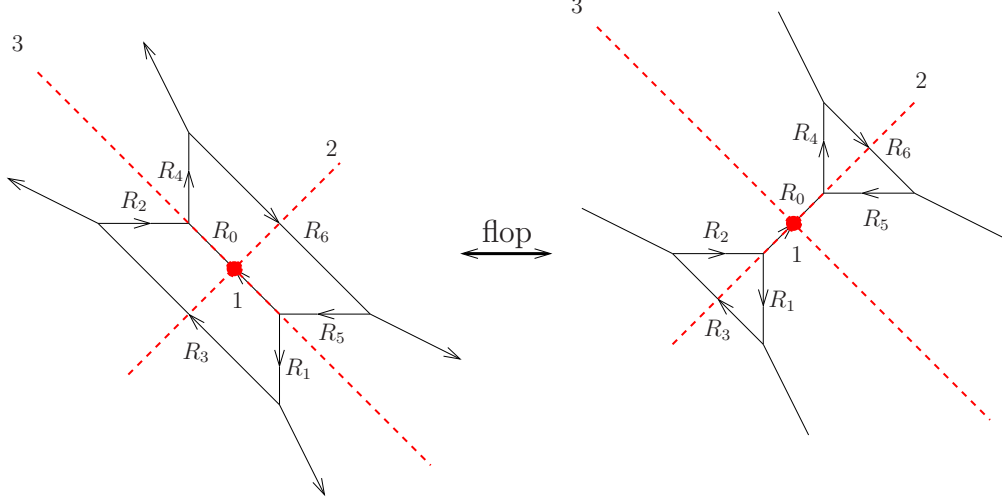


Figure 13: The involutive \mathbb{Z}_2 symmetries of the butterfly and $[\mathbb{P}^2]^2$.

with $R = \{R_1, R_3, R_5\}$ and

$$\begin{aligned} d(x) &= \ell(R_0)/2 + \ell(R_3), \\ d(y) &= \ell(R_1) + \ell(R_3) + \ell(R_5). \end{aligned} \quad (6.8)$$

Similarly, the point reflection of $[\mathbb{P}^2]^2$ (which has been already discussed in [4]) yields

$$Z_B^1 = \sum_{R, R_0=R_0^t} (-1)^{(\ell(R_0) \mp r(R_0))/2 - d(y)} q^{\kappa_{R_1} + \kappa_{R_2} + \kappa_{R_3}} C_{R_1 R_2^t R_0} C_{R_2 R_3^t} C_{R_3 R_1^t} \cdot x^{d(x)} y^{d(y)}, \quad (6.9)$$

with $R = \{R_1, R_2, R_3\}$,

$$\begin{aligned} d(x) &= \ell(R_0)/2, \\ d(y) &= \ell(R_1) + \ell(R_2) + \ell(R_3). \end{aligned} \quad (6.10)$$

We expand the resulting real free energies defined as in (3.4) into real Gopakumar-Vafa invariants ${}^{A/B}N_{d_x, d_y}^{(\chi)}$, following (6.1). We obtain the invariants listed in table 2 of appendix A. Note that the d_Q - χ -correlation holds in this example. For χ odd, we reproduce the results for $c = 1$, and for χ even, those for $c = 2$, of [4].

We observe that the real BPS numbers of the two phases are related via

$${}^A N_{d_x, d_y}^{(\chi)} = {}^B N_{2d_y - d_x, d_y}^{(\chi)}, \quad (6.11)$$

which is just (6.6) under the identification $d_y = d_z$. Note that in order that (6.11) hold exactly, *i.e.*, not only up to a sign, the pre-sign of the r -type sign needs to switch under the flop.

Involution 2

This involution acts as the identity on the moduli. The butterfly has three type 2 fixed edges (corresponding to three invariant S^1 's as fixed-point locus), such that we have to insert three c -type signs. According to the rules in section 3.3, there are two consistent global choices. We prefer the following expression:

$$Z_A^2 = \sum_R (-1)^{(\ell(R_0) \pm c(R_0) + \ell(R_3) \mp c(R_3) + \ell(R_6) \mp c(R_6^t))/2} q^{-\kappa_{R_0}/4 + \kappa_{R_1}/2 + \kappa_{R_3}/4 + \kappa_{R_5}/2 + 3\kappa_{R_6}/4} \\ \times C_{R_5^t R_1 R_0} C_{R_5 R_6^t} C_{R_3 R_1^t} \cdot x^{d(x)} y^{d(y)} z^{d(z)}, \quad (6.12)$$

with $R = \{R_0, R_1, R_3, R_5, R_6\}$ and

$$d(x) = \ell(R_0)/2 + \ell(R_3)/2 + \ell(R_6)/2, \\ d(y) = \ell(R_1) + \ell(R_3)/2, \\ d(z) = \ell(R_5) + \ell(R_6)/2. \quad (6.13)$$

Expansion of the partition function into real Gopakumar-Vafa invariants as in (6.1) delivers the invariants listed in table 3 of the appendix.

Turning to phase B, we have two type 2 fixed legs and two real vertices connected via an (isolated) type 3 fixed leg (see figure 13). Thus, we need to insert two c -type signs and make the right choice between straight and twisted real vertex. The rules of section 3.3 allow

$$Z_B^2 = \sum_{R, R_0=R_6^t} (-1)^{\ell(R_1) + \ell(R_4) + (\ell(R_0) \mp r(R_0) + \ell(R_3) \pm c(R_3) + \ell(R_6) \pm c(R_6^t))/2} \\ \times q^{5\kappa_{R_1}/4 + \kappa_{R_3}/4 + 5\kappa_{R_4}/4 + \kappa_{R_6}/4} \times C_{R_3 R_1^t} C_{R_6 R_4^t} C_{R_1 R_0}^{\text{real}} \tilde{C}_{R_4 R_0}^{\text{real}} x^{d(x)} y^{d(y)} z^{d(z)}, \quad (6.14)$$

with $R = \{R_1, R_3, R_4, R_6\}$ and

$$d(x) = \ell(R_0)/2, \\ d(y) = \ell(R_1) + \ell(R_3)/2, \\ d(z) = \ell(R_4) + \ell(R_6)/2. \quad (6.15)$$

But we wish to emphasize that exchanging $c(R_i)$ with $c(R_i^t)$ and straight with twisted real vertex gives the same result. Expansion gives the real Gopakumar-Vafa invariants listed in table 4 in the appendix. Since all moduli are mapped to themselves, we expect that the relation (6.6) persists, *i.e.*,

$${}^A N_{d_x, d_y, d_z}^{(\chi)} = {}^B N_{d_y + d_z - d_x, d_y, d_z}^{(\chi)}. \quad (6.16)$$

As we infer by comparing tables 3 and 4, this is indeed the case. Another check on the consistency of the obtained invariants is given by the relations

$$\begin{aligned} {}^A N_{d,0,d}^{(x)} &= {}^A N_{d,d,0}^{(x)} = \mathbb{P}^2 N_d^{(x)} , \\ {}^B N_{0,d,0}^{(x)} &= {}^B N_{0,0,d}^{(x)} = \mathbb{P}^2 N_d^{(x)} , \end{aligned} \tag{6.17}$$

counting the real invariants of the individual \mathbb{P}^2 in the geometry.

Involution 3

Similarly to involution 1, this involution projects the Kähler parameters to $y = z$. In fact, from a quotient space perspective of the action on $[\mathbb{P}^2]^2$, the only difference to involution 1 acting on $[\mathbb{P}^2]^2$ lies in the action on the central \mathbb{P}^1 . Whereas involution 1 acts without fixed-point on the \mathbb{P}^1 , involution 3 has an S^1 fixed locus. Since locally around the fixed-point locus the geometry corresponds to the conifold, and following the discussion of section 3, we expect that involution 3 yields the same real Gopakumar-Vafa invariants as involution 1.

Indeed, the orientifold partition function, where we inserted a single c -type sign for the type 2 fixed-leg, is given by

$$Z_B^3 = \sum_{R, R_0} (-1)^{d(y) + (\ell(R_0) \mp c(R_0))/2} q^{-\kappa_{R_0}/4 + \kappa_{R_1} + \kappa_{R_2} + \kappa_{R_3}} C_{R_1 R_2^t R_0} C_{R_2 R_3^t} C_{R_3 R_1^t} x^{d(x)} y^{d(y)} , \tag{6.18}$$

with $R = \{R_1, R_2, R_3\}$ and

$$\begin{aligned} d(x) &= \ell(R_0)/2 , \\ d(y) &= \ell(R_1) + \ell(R_2) + \ell(R_3) . \end{aligned} \tag{6.19}$$

The resulting free energy is equal to that of involution 1, as expected. For involution 3 acting on the butterfly we obtain

$$\begin{aligned} Z_A^3 &= \sum_{R_0=R_0^t, R} (-1)^{(\ell(R_0) \pm r(R_0))/2 - \ell(R_3)} q^{3\kappa_{R_1}/4 + \kappa_{R_2}/4 + \kappa_{R_3}/2} x^{d(x)} y^{d(y)} \\ &\quad \times C_{R_2 R_3^t} C_{R_3 R_1^t} C_{R_2^t R_0}^{\text{real}} \tilde{C}_{R_1^t R_0}^{\text{real}} , \end{aligned} \tag{6.20}$$

with $R = \{R_1, R_2, R_3\}$ as before and

$$\begin{aligned} d(x) &= \ell(R_0)/2 + \ell(R_3) , \\ d(y) &= \ell(R_1) + \ell(R_2) + \ell(R_3) . \end{aligned} \tag{6.21}$$

Again, $Z_A^3 = Z_A^1$. Note that in order that the invariants of the two geometries agree exactly (including sign), the pre-signs of the r -type and c -type sign need to be opposite.

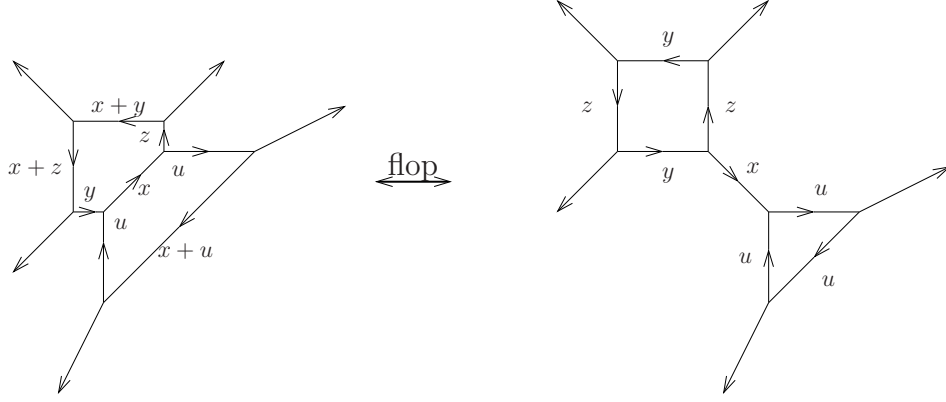


Figure 14: The (p, q) -webs of the hybridfly (left) and $[\mathbb{P}^2][\mathbb{F}_0]$ (right) geometry with Kähler moduli associated to the edges. The two geometries are related via a flop of the central \mathbb{P}^1 .

6.2 Hybridfly

The next more complicated example is the 4-parameter geometry shown in the left of figure 14. We will refer to it as hybridfly. The flopped geometry is a \mathbb{P}^2 connected to a \mathbb{F}_0 via a conifold. We therefore denote the flopped geometry as $[\mathbb{F}_0][\mathbb{P}^2]$. We will also refer to the hybridfly as phase A and to $[\mathbb{F}_0][\mathbb{P}^2]$ as phase B .

Closed string geometry

The corresponding (closed) topological string partition functions can be easily obtained to be given by (see figure 15 for the association of representations to edges)

$$\begin{aligned}
Z_A = & \sum_R (-1)^{\ell(R_0) + \ell(R_1) + \ell(R_4) - \ell(R_6)} q^{(-\kappa_{R_2} - \kappa_{R_3} + \kappa_{R_5} + 2\kappa_{R_6} + \kappa_{R_7})/2} x^{d(x)} y^{d(y)} z^{d(z)} u^{d(u)} \\
& \times C_{R_1 R_5 R_0^t} C_{R_1^t R_2} C_{R_2^t R_3} C_{R_3^t R_4} C_{R_7^t R_4^t R_0} C_{R_7 R_6^t} C_{R_6 R_5^t} ,
\end{aligned} \tag{6.22}$$

with $R = \{R_0, \dots, R_7\}$ and

$$\begin{aligned}
d(x) &= \ell(R_0) + \ell(R_2) + \ell(R_3) + \ell(R_6) , \\
d(y) &= \ell(R_2) + \ell(R_4) , \\
d(z) &= \ell(R_1) + \ell(R_3) , \\
d(u) &= \ell(R_5) + \ell(R_6) + \ell(R_7) .
\end{aligned} \tag{6.23}$$

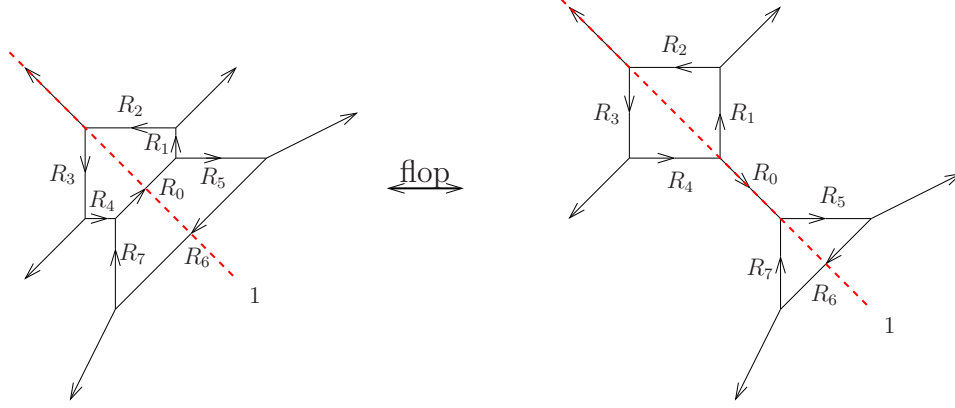


Figure 15: The single involutive \mathbb{Z}_2 symmetry of the hybridfly and $[\mathbb{F}_0][\mathbb{P}^2]$.

Similarly, we obtain for the flopped geometry

$$\begin{aligned}
Z_B &= \sum_R (-1)^{\ell(R_0) - d(u)} q^{-(\kappa_{R_1} + \kappa_{R_2} + \kappa_{R_3} + \kappa_{R_4})/2} q^{\kappa_{R_5} + \kappa_{R_6} + \kappa_{R_7}} x^{d(x)} y^{d(y)} z^{d(z)} u^{d(u)} \\
&\times C_{R_4^t R_1 R_0} C_{R_1^t R_2} C_{R_2^t R_3} C_{R_3^t R_4} C_{R_5 R_7^t R_0^t} C_{R_6 R_5^t} C_{R_7 R_6^t},
\end{aligned} \tag{6.24}$$

with

$$\begin{aligned}
d(x) &= \ell(R_0), \\
d(y) &= \ell(R_2) + \ell(R_4), \\
d(z) &= \ell(R_1) + \ell(R_3), \\
d(u) &= \ell(R_5) + \ell(R_6) + \ell(R_7).
\end{aligned} \tag{6.25}$$

The relation between the Gopakumar-Vafa invariants ${}^{A/B}n_{d_x, d_y, d_z, d_u}^{(g)}$ of the two geometries reads

$${}^A n_{d_x, d_y, d_z, d_u}^{(g)} = {}^B n_{d_y + d_z + d_u - d_x, d_y, d_z, d_u}^{(g)}. \tag{6.26}$$

These two geometries have only one involutive symmetry, as indicated in figure 15.

Involution 1

Let us start with the hybridfly. The involution projects the moduli $y = z$ and maps the remaining two moduli to themselves. We need to insert two c -type signs and one real vertex.

$$\begin{aligned}
Z_A^1 &= \sum_R (-1)^{(\ell(R_0) \pm c(R_0^t) + \ell(R_6) \pm c(R_6^t))/2 + \ell(R_1)} q^{(\kappa_{R_0} - 3\kappa_{R_2} + 2\kappa_{R_5} + \kappa_{R_6})/4} \\
&\times C_{R_1 R_5 R_0^t} C_{R_1^t R_2} C_{R_6 R_5^t} C_{R_2^t}^{\text{real}} x^{d(x)} z^{d(z)} u^{d(u)},
\end{aligned} \tag{6.27}$$

with $R = \{R_0, R_1, R_2, R_5, R_6\}$ and

$$\begin{aligned} d(x) &= \ell(R_0)/2 + \ell(R_2) + \ell(R_6)/2, \\ d(z) &= \ell(R_1) + \ell(R_2), \\ d(u) &= \ell(R_5) + \ell(R_6)/2. \end{aligned} \tag{6.28}$$

The real Gopakumar-Vafa invariants extracted from the corresponding free energy are listed in table 5 of the appendix.

In the flopped phase, we obtain

$$\begin{aligned} Z_B^1 &= \sum_{R, R_0=R_0^t} (-1)^{(\ell(R_0 \mp r(R_0))/2 + \ell(R_5) + (\ell(R_6) \pm c(R_6))/2)} q^{(-\kappa_{R_1} - 3\kappa_{R_2} + 5\kappa_{R_5} - \kappa_{R_6})/4} \\ &\quad \times C_{R_1^t R_2} \cdot C_{R_6 R_5^t} \cdot C_{R_2^t}^{\text{real}} \cdot \tilde{C}_{R_1^t R_0}^{\text{real}} \cdot C_{R_5 R_0}^{\text{real}} x^{d(x)} z^{d(z)} u^{d(u)} \end{aligned} \tag{6.29}$$

with $R = \{R_1, R_2, R_5, R_6\}$ and

$$\begin{aligned} d(x) &= \ell(R_0)/2, \\ d(z) &= \ell(R_1) + \ell(R_2), \\ d(u) &= \ell(R_5) + \ell(R_6)/2. \end{aligned} \tag{6.30}$$

The Gopakumar-Vafa invariants are listed in table 6. The relation to the numbers in table 5 is

$${}^A N_{d_x, d_z, d_u}^{(\chi)} = {}^B N_{2d_z + d_u - d_x, d_z, d_u}^{(\chi)}. \tag{6.31}$$

As a consistency check on the obtained invariants, we recover

$$\begin{aligned} {}^A N_{0,0,d}^{(\chi)} &= {}^B N_{d,0,d}^{(\chi)} = \mathbb{P}^2 N_d^{(\chi)}, \\ {}^A N_{0,d,0}^{(\chi)} &= {}^B N_{2d,d,0}^{(\chi)} = \mathbb{F}_0 N_d^{(\chi)}, \end{aligned} \tag{6.32}$$

i.e., the real invariants of the \mathbb{P}^2 and \mathbb{F}_0 in the geometry. Note that Z^1 of \mathbb{F}_0 can be easily obtained by setting $R_5 = R_6 = R_0 = \cdot$ in (6.29). The resulting real invariants are listed in table 1.

We note that the last non-vanishing invariants for fixed d in table 1 show a very simple structure:

$$\mathbb{F}_0 N_d^{(d-1)^2-1} = 1, \quad \text{for } d \text{ even}; \quad \mathbb{F}_0 N_d^{(d-1)^2-2} = 2, \quad \text{for } d \text{ odd}. \tag{6.33}$$

These results can be verified in the computational scheme for GV invariants developed in [25]. In the notation of section 8.4 of that reference, we are interested in the real

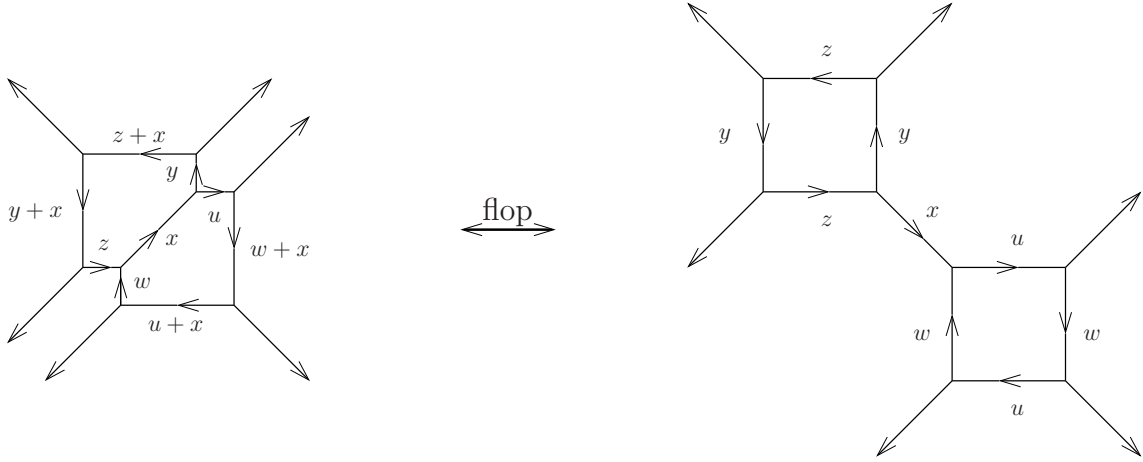


Figure 16: The (p, q) -webs of the pentafly (left) and $[\mathbb{F}_0]^2$ (right) with Kähler moduli associated to the edges. The geometries are related via a flop of the central \mathbb{P}^1 .

version of n_d^r with the maximal possible value of r for fixed d . (Our d is $a = b$ of [25], and $\chi = r - 1$.) For a even, we have $r = (a - 1)^2$, and the relevant moduli space is $\mathbb{P}^{(a+1)^2-1}$, with $e(\mathbb{R}\mathbb{P}^{\text{even}}) = 1$. For a odd, on the other hand, since $e(\mathbb{R}\mathbb{P}^{\text{odd}}) = 0$, we need to look at $\delta = 1$, *i.e.*, $r = (a - 1)^2 - 1$. Then by the first line of equation (5.4), we need $e(\mathcal{C})$, where \mathcal{C} is the universal curve. $\mathcal{C} \rightarrow \mathbb{P}^1 \times \mathbb{P}^1$ with fiber $\mathbb{P}^{(a+1)^2-2}$. Because the involution exchanges the two \mathbb{P}^1 's, we have $e(\mathcal{C}^{\text{real}}) = e(\mathbb{R}\mathbb{P}^{(a+1)^2-2}) \cdot e(\mathbb{C}\mathbb{P}^1) = 2$.

6.3 Pentafly

As a final example, we consider the 5-parameter geometries shown in figure 16, which are again related via a flop of the central \mathbb{P}^1 .

Closed string

The geometry in the left of the figure will be denoted as pentafly, and the flopped geometry as $[\mathbb{F}_0]^2$, since this geometry consists of two \mathbb{F}_0 connected via a conifold. We will refer to the pentafly also as phase A and to $[\mathbb{F}_0]^2$ as phase B . Note that phase A consists of two \mathcal{B}_2 . Here, \mathcal{B}_2 denotes the 2-point blowup of \mathbb{P}^2 . Thus, we expect to recover at specific values in parameter space the known results of \mathbb{P}^2 .

The corresponding (closed) topological string partition functions can be easily obtained (see figure 17 for the association of representations to edges). We infer for the

pentally,

$$\begin{aligned}
Z_A = & \sum_R (-1)^{\ell(R_0)+\ell(R_1)+\ell(R_4)+\ell(R_5)+\ell(R_8)} q^{(-\kappa_{R_2}-\kappa_{R_3}+\kappa_{R_6}+\kappa_{R_7})/2} \\
& \times x^{d(x)} y^{d(y)} z^{d(z)} u^{d(u)} w^{d(w)} \\
& \times C_{R_1 R_5 R_0^t} C_{R_1^t R_2} C_{R_2^t R_3} C_{R_3^t R_4} C_{R_8^t R_4 R_0} C_{R_5^t R_6} C_{R_6^t R_7} C_{R_7^t R_8} ,
\end{aligned} \tag{6.34}$$

with $R = \{R_0, \dots, R_8\}$ and

$$\begin{aligned}
d(x) &= \ell(R_0) + \ell(R_2) + \ell(R_3) + \ell(R_6) + \ell(R_7) , \\
d(y) &= \ell(R_1) + \ell(R_3) , \\
d(z) &= \ell(R_2) + \ell(R_4) , \\
d(u) &= \ell(R_5) + \ell(R_7) , \\
d(w) &= \ell(R_6) + \ell(R_8) .
\end{aligned} \tag{6.35}$$

Meanwhile, the partition function of $[\mathbb{F}_0]^2$ reads

$$\begin{aligned}
Z_B = & \sum_R (-1)^{d(x)} q^{-(\kappa(R_1)+\kappa(R_2)+\kappa(R_3)+\kappa(R_4))/2} q^{(\kappa_{R_5}+\kappa_{R_6}+\kappa_{R_7}+\kappa_{R_8})/2} \\
& \times x^{d(x)} y^{d(y)} z^{d(z)} u^{d(u)} w^{d(w)} \\
& \times C_{R_4^t R_1 R_0} C_{R_1^t R_2} C_{R_2^t R_3} C_{R_3^t R_4} C_{R_6 R_5^t} C_{R_5 R_8^t R_0} C_{R_7 R_6^t} C_{R_8 R_7^t} ,
\end{aligned} \tag{6.36}$$

with

$$\begin{aligned}
d(x) &= \ell(R_0) , \\
d(y) &= \ell(R_1) + \ell(R_3) , \\
d(z) &= \ell(R_2) + \ell(R_4) , \\
d(u) &= \ell(R_5) + \ell(R_7) , \\
d(w) &= \ell(R_6) + \ell(R_8) .
\end{aligned} \tag{6.37}$$

The relation between the Gopakumar-Vafa invariants ${}^{A/B}n_{d_x, d_y, d_z, d_u, d_w}^{(g)}$ under the flop transition relating phase A and B is

$${}^A n_{d_x, d_y, d_z, d_u, d_w}^{(g)} = {}^B n_{d_y+d_z+d_u+d_w-d_x, d_y, d_z, d_u, d_w}^{(g)} . \tag{6.38}$$

The two geometries possess three involutive \mathbb{Z}_2 symmetries which we illustrated in figure 17. For each involution, we discuss in the following the respective orientifold topological partition function.

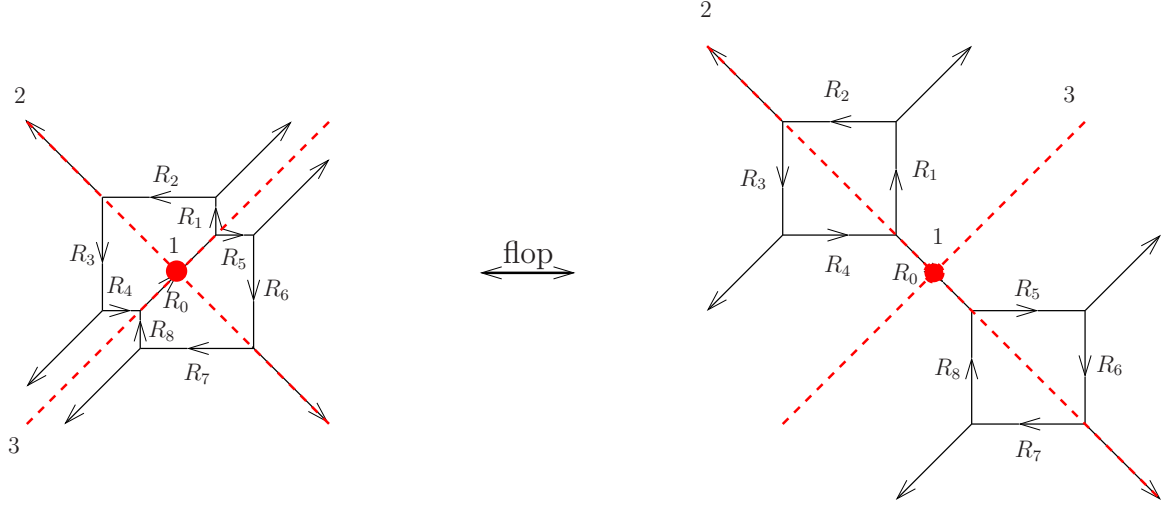


Figure 17: The involutive \mathbb{Z}_2 symmetries of the pentafly and $[\mathbb{F}_0]^2$.

Involution 1

The point-reflection acts via identifying $y = w$ and $z = u$, while x is mapped to itself. We deduce that the real partition function of the pentafly reads

$$Z_A^1 = \sum_{R, R_0=R_0^t} (-1)^{(\ell(R_0) \pm r(R_0))/2 + \ell(R_1) + \ell(R_4)} q^{-(\kappa_{R_2} + \kappa_{R_3})/2} x^{d(x)} y^{d(y)} z^{d(z)} \quad (6.39)$$

$$\times C_{R_1 R_4 R_0^t} C_{R_1^t R_2} C_{R_2^t R_3} C_{R_3^t R_4},$$

with $R = \{R_1, \dots, R_4\}$ and

$$\begin{aligned} d(x) &= \ell(R_0)/2 + \ell(R_2) + \ell(R_3), \\ d(y) &= \ell(R_1) + \ell(R_3), \\ d(z) &= \ell(R_2) + \ell(R_4). \end{aligned} \quad (6.40)$$

Similarly, we obtain for $[\mathbb{F}_0]^2$

$$Z_B^1 = \sum_{R, R_0=R_0^t} (-1)^{(\ell(R_0) \mp r(R_0))/2} q^{-(\kappa_{R_1} + \kappa_{R_2} + \kappa_{R_3} + \kappa_{R_4})/2} x^{d(x)} y^{d(y)} z^{d(z)} \quad (6.41)$$

$$\times C_{R_4^t R_1 R_0} C_{R_1^t R_2} C_{R_2^t R_3} C_{R_3^t R_4},$$

with R as for the pentafly and

$$\begin{aligned} d(x) &= \ell(R_0)/2, \\ d(y) &= \ell(R_1) + \ell(R_3), \\ d(z) &= \ell(R_2) + \ell(R_4). \end{aligned} \quad (6.42)$$

As usual for this type of involution, we inserted a single r -type sign into the projected partition functions.

We expand both partition functions into real Gopakumar-Vafa invariants and list the results in tables 7 and 8. The invariants of both phases are related via (in order to match the signs, we invert the r -type sign under the flop)

$${}^A N_{d_x, d_y, d_z}^{(\chi)} = {}^B N_{2d_y + 2d_z - d_x, d_y, d_z}^{(\chi)} . \quad (6.43)$$

Involution 2

From figure 17 we infer that this involution projects the Kähler parameters to $x = y$ and $u = w$. The real topological string partition function is

$$\begin{aligned} Z_A^2 = & \sum_R (-1)^{(\ell(R_0) \mp c(R_0))/2 + \ell(R_1) + \ell(R_5)} q^{(\kappa_{R_0} - 3\kappa_{R_2} + \kappa_{R_6})/4} x^{d(x)} y^{d(y)} u^{d(u)} \\ & \times C_{R_1 R_5 R_0^t} C_{R_1^t R_2} C_{R_6 R_5^t} C_{R_2^t}^{\text{real}} \tilde{C}_{R_6}^{\text{real}} , \end{aligned} \quad (6.44)$$

with $R = \{R_0, R_1, R_2, R_5, R_6\}$ and

$$\begin{aligned} d(x) &= \ell(R_0)/2 + \ell(R_2) + \ell(R_6) , \\ d(y) &= \ell(R_1) + \ell(R_2) , \\ d(u) &= \ell(R_5) + \ell(R_6) . \end{aligned} \quad (6.45)$$

Expansion of the resulting free energies yields the invariants listed in table 9. Note that since the pentaflly consists of two \mathcal{B}_2 's, we expect to recover the real Gopakumar-Vafa invariants ${}^{\mathcal{B}_2} N_{d_x, d_y}^{(\chi)}$ of \mathcal{B}_2 . Setting $R_5 = R_6 = \cdot$ in (6.44) and (6.45), the partition function reduces to the partition function of real \mathcal{B}_2 and the resulting invariants indeed satisfy

$${}^B N_{d_x, d_y, 0}^{(\chi)} = {}^B N_{d_x, 0, d_y}^{(\chi)} = {}^{\mathcal{B}_2} N_{d_x, d_y}^{(\chi)} . \quad (6.46)$$

A non-trivial check on the consistency of the obtained invariants lies in the fact that we recover the known invariants of local \mathbb{P}^2 , *i.e.*,

$${}^{\mathcal{B}_2} N_{d_x, d_x}^{(\chi)} = \mathbb{P}^2 N_{d_x}^{(\chi)} . \quad (6.47)$$

Let us turn to the flopped geometry.

$$\begin{aligned} Z_B^2(\sigma, \tau) = & \sum_{R, R_0=R_0^t} (-1)^{(\ell(R_0) \mp r(R_0))/2} q^{(-\kappa_{R_1} - 3\kappa_{R_2} + 3\kappa_{R_5} + \kappa_{R_6})/4} x^{d(x)} y^{d(y)} u^{d(u)} \\ & \times C_{R_1^t R_2} C_{R_6 R_5^t} C_{R_2^t}^{\text{real}} \tilde{C}_{R_1^t R_0}^{\text{real}} C_{R_5 R_0}^{\text{real}} \tilde{C}_{R_6}^{\text{real}} , \end{aligned} \quad (6.48)$$

with $R = \{R_1, R_2, R_5, R_6\}$ and

$$\begin{aligned} d(x) &= \ell(R_0)/2, \\ d(y) &= \ell(R_1) + \ell(R_2), \\ d(u) &= \ell(R_5) + \ell(R_6). \end{aligned} \tag{6.49}$$

The invariants are listed in table 10.

Similarly as for the pentaflly, setting $R_5 = R_6 = \cdot$, we calculate the partition function of a flop of real \mathcal{B}_2 , which is \mathbb{F}_0 with a conifold attached. We recover the invariants of the two \mathbb{F}_0 in the geometry as follows

$${}^B N_{0,d,0}^{(\chi)} = {}^B N_{0,0,d}^{(\chi)} = \mathbb{F}_0 N_d^{(\chi)}. \tag{6.50}$$

Also, the invariants of the two phases are related via

$${}^A N_{d_x, d_y, d_u}^{(\chi)} = {}^B N_{2d_y + 2d_u - d_x, d_y, d_u}^{(\chi)}, \tag{6.51}$$

as expected.

Involution 3

The projected partition function of the pentaflly under involution 3 is given by

$$\begin{aligned} Z_A^3 &= \sum_{R, R_0=R_0^t} (-1)^{(\ell(R_0) \pm r(R_0))/2 + \ell(R_1) + \ell(R_4)} q^{-(\kappa_{R_2} + \kappa_{R_3})/2 + (\kappa_{R_1} - \kappa_{R_4})/4} \\ &\quad \times C_{R_1^t R_2} \cdot C_{R_2^t R_3} \cdot C_{R_3^t R_4} \cdot C_{R_1 R_0}^{\text{real}} \tilde{C}_{R_4 R_0}^{\text{real}} x^{d(x)} y^{d(y)} z^{d(z)}, \end{aligned} \tag{6.52}$$

with $R = \{R_1, \dots, R_4\}$,

$$\begin{aligned} d(x) &= \ell(R_0)/2 + \ell(R_2) + \ell(R_3), \\ d(y) &= \ell(R_1) + \ell(R_3), \\ d(z) &= \ell(R_2) + \ell(R_4). \end{aligned} \tag{6.53}$$

When expanding the partition function according to (6.1), we notice that while the ${}^X N_{d_x d_y d_z}^{(\chi)}$ are all integer, they *do not* satisfy the d_Q - χ correlation prominent in all previous examples (here, $d_Q = d_x$). This is somewhat unexpected, but in fact not in violation of any fundamental principle. The simplest geometry with this feature is the closed topological vertex of [26].

Let us compare to the flopped $[\mathbb{F}_0]^2$ geometry. The projected partition function is given by

$$Z_B^3 = \sum_R (-1)^{(\ell(R_0)+c(R_0))/2} q^{-\kappa_{R_0}/4 - (\kappa_{R_1} + \kappa_{R_2} + \kappa_{R_3} + \kappa_{R_4})/2} x^{d(x)} y^{d(y)} z^{d(z)} \times C_{R_4^t R_1 R_0} C_{R_1^t R_2} C_{R_2^t R_3} C_{R_3^t R_4}, \quad (6.54)$$

Again, the expansion shows a violation of d_Q - χ correlation. The terms that do satisfy the correlation coincide to those of involution 1, while all terms are related to those of the pentaflly via the flop (6.43).

We note that the terms that violate d_Q - χ correlation change sign under the replacement of C^{real} with \tilde{C}^{real} and $c(R)$ with $c(R^t)$, while those that satisfy d_Q - χ correlation are invariant under this replacement. We can write this in terms of the formula

$$Z(q^{1/2}, Q^{1/2}, Q) = \tilde{Z}(-q^{1/2}, -Q^{1/2}, Q'), \quad (6.55)$$

where Z and \tilde{Z} are the partition functions evaluated with the two consistent real vertex prescriptions discussed in section 3.3.

7 Conclusions

In this paper, we have developed the real topological vertex formalism proposed in [2] to a complete computational prescription for the evaluation of real topological string amplitudes on local toric Calabi-Yau threefolds. The real vertex is essentially a squareroot of the ordinary vertex amplitude of [1]. We have uncovered several new sign subtleties that arise in the gluing of the real vertex to the global expression. In particular, we have seen that we actually require two different real vertices with slightly different sign insertions.

We have also discussed the interpretation of the real vertex in Chern-Simons theory on the orbifold S^3/\mathbb{Z}_2 with fixed point locus in codimension two, giving a complete realization of the existence of the two types of real vertex. We have also given an interpretation via the melting crystal picture of [9], which consists in considering a symmetrically melting crystal. Via this connection, we have made and studied a proposal for the constant map contribution to real topological string on general Calabi-Yau orientifolds.

Among the few open questions, let us mention just two: It would be interesting to study also the melting crystal representation of the real vertex with non-trivial

representation on the fixed leg (non-trivial asymptotics along the x_2 -axis). It is rather straightforward to write down the vertex operator formula, but it is not immediately clear how to relate the resulting expressions with the squareroots in (3.29) and (3.30).

We have seen in the final example in section 6 that there are cases in which the real topological partition function does not satisfy “ d_Q - χ correlation” (see beginning of section 6 for the definition of this notion). This correlation might have been expected based on the experience with real localization techniques [3, 2]. In particular, local tadpole cancellation was implemented in this context by cancelling even degree real maps between holes and crosscaps on the worldsheet, and by neglecting any possible contribution from a non-trivial intersection theory on the moduli space of real curves. (The only Hodge integrals required for the computations in [2] are those on moduli spaces of complex curves.) The violation of d_Q - χ correlation from the real topological vertex seems to indicate that this assumption might not be correct in general. It would be interesting to pursue this further.

Acknowledgments We would like to thank Marcos Mariño for Chern-Simons consultations at initial stages of this work, and in particular for reminding us of Hořava’s work. We thank Chris Beasley, Jim Bryan, and Cumrun Vafa for valuable discussions. The work of D.K. was supported in part by an EU Marie-Curie EST fellowship, the Max-Planck society and the WPIRC initiative by MEXT of Japan. D.K. thanks the ASC at LMU and CERN for hospitality during part of this project. S.P. thanks ASC at LMU for hospitality. J.W. is grateful to McGill University and to SUNY Stonybrook during the 2009 Simons Workshop for hospitality while some of the signs of this work were being fixed.

A Real Gopakumar-Vafa invariants

d/χ	0	1	2	3	4	5	6	7	8
0			1	8	69	608	5475	50136	465173
2				2	76	1544	24696	382934	5324640
4					39	2020	65892	1651424	35161960
6					10	1586	111660	4914874	164667808
8				1	756	132105	132105	10723220	582872279
10						212	111774	17629822	1607349528
12						32	68342	22182896	3518490422
14						2	30194	21562774	6195809584
16							9530	16278148	8866082190
18							2092	9561340	10391531036
20							303	4361964	10036474120
22							26	1536200	8023729064
24							1	412728	5325069376
26								82898	2937580602
28								12036	1346409352
30								1192	511497566
32								72	160302439
34								2	41130990
36									8542684
38									1412510
40									181428
42									17436
44									1179
46									50
48									1
50									

Table 1: $\mathbb{F}_0 N_d^{(\chi)}$ of the diagonal involution of \mathbb{F}_0 (two real vertices).

The vectors in the following tables are to be understood as a list of real Gopakumar-Vafa invariants for higher χ . When the invariants satisfy the $d_Q-\chi$ correlation, we only list the values for $\chi \equiv \sum_A d_{Q_A} \pmod 2$, since the remaining invariants are identically zero. The first entry in each list corresponds to $\chi = -1$, or $\chi = 0$. When the last entry of the list is zero, all invariants of higher χ also vanish. (Otherwise, the list might be truncated to fit into the table.)

$d_x \setminus d_y$	0	1	2	3	4
0	0	0	0	0	0
1	-1	-2	-3	-4	-5
2	0	0	0	$-(0, 1, 0)$	$-(0, 2, 0)$
3	0	0	5	$(30, 7, 0)$	$(112, 59, 9, 0)$
4	0	0	0	4	$(0, 11, 6, 1, 0)$
5	0	0	0	$-(32, 9, 0)$	$-(369, 315, 103, 12)$
6	0	0	0	0	0
7	0	0	0	0	$(286, 288, 108, 14)$
8	0	0	0	0	0

$d_x \setminus d_y$	0	1	2	3	4
0	0	0	0	0	0
1	1	-2	5	$-(32, 9, 0)$	$(286, 288, 108, 14)$
2	0	0	0	0	0
3	0	0	-3	$(30, 7, 0)$	$-(369, 315, 103, 12)$
4	0	0	0	$-(0, 1, 0)$	$(0, 11, 6, 1, 0)$
5	0	0	0	-4	$(112, 59, 9, 0)$
6	0	0	0	0	$-(0, 2, 0)$
7	0	0	0	0	-5
8	0	0	0	0	0

Table 2: Left table: $A N_{d_x, d_y}^{(\chi)}$ for involution 1 & 3 of the butterfly. Right table: $B N_{d_x, d_y}^{(\chi)}$ of the corresponding $[\mathbb{P}^2]^2$ involutions.

$\frac{d_x=0}{d_y/d_z}$	0	1	2	3	4	5	6
0	0	0	0	0	0	0	0
1	0	0	0	0	0	0	0
2	0	0	0	0	0	0	0
3	0	0	0	0	0	0	0
4	0	0	0	0	0	0	0
5	0	0	0	0	0	0	0
6	0	0	0	0	0	0	0

$\frac{d_x=1}{d_y/d_z}$	0	1	2	3	4	5	6
0	-1	-1	-1	-1	-1	-1	-1
1	-1	0	0	0	0	0	0
2	-1	0	-1	-1	-1	-1	-1
3	-1	0	-1	0	0	0	0
4	-1	0	-1	0	-1	-1	-1
5	-1	0	-1	0	-1	0	0
6	-1	0	-1	0	-1	0	-1

$\frac{d_x=2}{d_y/d_z}$	0	1	2	3	4	5	6
0	0	0	0	(0, 1, 0)	0	(0, 4, 1, 0)	0
1	0	0	0	0	0	0	0
2	0	0	0	(0, 1, 0)	0	(0, 5, 1, 0)	0
3	(0, 1, 0)	0	(0, 1, 0)	(0, 1, 0)	(0, 1, 0)	(0, 1, 0)	(0, 1, 0)
4	0	0	0	(0, 1, 0)	0	(0, 5, 1, 0)	0
5	(0, 4, 1, 0)	0	(0, 5, 1, 0)	(0, 1, 0)	(0, 5, 1)	(0, 5, 1, 0)	(0, 5, 1)
6	0	0	0	(0, 1, 0)	0	(0, 5, 1, 0)	0

$\frac{d_x=3}{d_y/d_z}$	0	1	2	3	4	5	6
0	0	0	0	1	2	(5, 1, 0)	(9, 2, 0)
1	0	0	0	0	0	0	0
2	0	0	1	2	(6, 1, 0)	(11, 2, 0)	(22, 8, 1, 0)
3	1	0	2	-(0, 1, 0)	4	-(0, 5, 1, 0)	6
4	2	0	(6, 1, 0)	4	(18, 7, 1, 0)	(18, 3, 0)	(48, 30, 9, 1, 0)
5	(5, 1, 0)	0	(11, 2, 0)	-(0, 5, 1, 0)	(18, 3, 0)	-(0, 22, 9, 1, 0)	(30, 5, 0)
6	(9, 2, 0)	0	(22, 8, 1, 0)	6	(48, 30, 9, 1, 0)	(30, 5, 0)	(103, 94, 46, 11, 1, 0)

$\frac{d_x=4}{d_y/d_z}$	0	1	2	3	4	5	6
0	0	0	0	0	(0, 3, 1, 0)	-(0, 4, 1, 0)	(0, 35, 57, 36, 10, 1, 0)
1	0	0	0	0	0	0	0
2	0	0	0	0	-(0, 1, 0)	-(0, 18, 8, 1, 0)	(0, 34, 57, 36, 10, 1, 0)
3	0	0	-(0, 1, 0)	-(0, 2, 0)	-(0, 6, 1, 0)	-(0, 11, 2, 0)	-(0, 22, 8, 1, 0)
4	(0, 3, 1, 0)	0	0	-(0, 6, 1, 0)	-(0, 9, 6, 1, 0)	-(0, 60, 38, 10, 1, 0)	-(0, 27, 26, 9, 1, 0)
5	-(0, 4, 1, 0)	0	-(0, 18, 8, 1, 0)	-(0, 11, 2, 0)	-(0, 60, 38, 10, 1, 0)	-(0, 60, 21, 2, 0)	-(0, 165, 138, 57, 12, 1, 0)
6	(0, 35, 57, 36, 10, 1, 0)	0	(0, 34, 57, 36, 10, 1, 0)	-(0, 22, 8, 1, 0)	-(0, 27, 26, 9, 1, 0)	-(0, 165, 138, 57, 12, 1, 0)	-(0, 153, 252, 182, 68, 13, 1, 0)

$\frac{d_x=5}{d_y/d_z}$	0	1	2	3	4	5	6
0	0	0	0	0	0	-(5, 10, 6, 1, 0)	-(14, 40, 57, 36, 10, 1, 0)
1	0	0	0	0	0	0	0
2	0	0	0	0	-2	-(10, 2, 0)	-(45, 54, 59, 36, 10, 1, 0)
3	0	0	0	(0, 1, 0)	-5	(0, 18, 8, 1, 0)	-(35, 42, 57, 36, 10, 1, 0)
4	0	0	-2	-5	-(27, 9, 1, 0)	-(42, 19, 27, 9, 1, 0)	-(192, 155, 88, 39, 10, 1, 0)
5	-(5, 10, 6, 1, 0)	0	-(10, 2, 0)	(0, 18, 8, 1, 0)	-(42, 19, 27, 9, 1, 0)	(0, 186, 169, 67, 13, 1, 0)	-(198, -24, 40, 17, 2, 0)
6	-(14, 40, 57, 36, 10, 1, 0)	0	-(45, 54, 59, 36, 10, 1, 0)	-(35, 42, 57, 36, 10, 1, 0)	-(192, 155, 88, 39, 10, 1, 0)	-(198, -24, 40, 17, 2, 0)	-(818, 852, 498, 179, 36, 3, 0)

$\frac{d_x=6}{d_y/d_z}$	0	1	2	3	4	5	6
0	0	0	0	0	0	0	-(0, 44, 63, 37, 10, 1, 0)
1	0	0	0	0	0	0	0
2	0	0	0	0	0	(0, 4, 1, 0)	-(0, 70, 114, 72, 20, 2, 0)
3	0	0	0	0	(0, 2, 0)	(0, 10, 2, 0)	(0, 45, 54, 59, 36, 10, 1, 0)
4	0	0	0	(0, 2, 0)	0	(0, 72, 45, 11, 1, 0)	-(0, 82, 174, 126, 38, 4, 0)
5	0	0	(0, 4, 1, 0)	(0, 10, 2, 0)	(0, 72, 45, 11, 1, 0)	-(0, -105, 41, 104, 54, 12, 1, 0)	(0, 570, 685, 521, 276, 89, 15, 1)
6	-(0, 44, 63, 37, 10, 1, 0)	0	-(0, 70, 114, 72, 20, 2, 0)	(0, 45, 54, 59, 36, 10, 1, 0)	-(0, 82, 174, 126, 38, 4, 0)	(0, 570, 685, 521, 276, 89, 15, 1)	(0, 36, -96, -88, -16, 4, 1, 0)

Table 3: $A_{d_x, d_y, d_z}^{(x)}$ for involution 2 of the butterfly.

$\frac{d_x=0}{d_y/d_z}$	0	1	2	3	4	5	6
0	0	-1	0	1	(0, 3, 1)	-(5, 10, 6)	-(0, 44, 63)
1	-1	0	0	0	0	0	0
2	0	0	0	0	0	0	0
3	1	0	0	0	0	0	0
4	(0, 3, 1)	0	0	0	0	0	0
5	-(5, 10, 6)	0	0	0	0	0	0
6	-(0, 44, 63)	0	0	0	0	0	0

$\frac{d_x=1}{d_y/d_z}$	0	1	2	3	4	5	6
0	1	0	-1	(0, 1, 0)	2	-(0, 4, 1)	-(14, 40, 57)
1	0	0	0	0	0	0	0
2	-1	0	1	-(0, 1, 0)	2	(0, 4, 1)	(14, 40, 57)
3	(0, 1, 0)	0	-(0, 1, 0)	(0, 1, 0)	(0, 2, 0)	-(0, 4, 1)	-(0, 14, 40)
4	2	0	-2	(0, 2, 0)	4	-(0, 8, 2)	-(28, 80, 114)
5	-(0, 4, 1, 0)	0	(0, 4, 1, 0)	-(0, 4, 1, 0)	-(0, 8, 2)	(16, 8, 1)	(0, 56, 174)
6	-(14, 40, 57)	0	(14, 40, 57)	-(0, 14, 40)	-(28, 80, 114)	(0, 56)	(196, 1120)

$\frac{d_x=2}{d_y/d_z}$	0	1	2	3	4	5	6
0	0	0	0	-1	0	(5, 1, 0)	(0, 35, 57, 36, 10, 1)
1	0	0	0	0	0	0	0
2	0	0	0	2	0	-(10, 2, 0)	-(0, 70, 114, 72, 20, 2)
3	-1	0	2	-(0, 2, 0)	-5	(0, 10, 2, 0)	(32, 79, 114, 72, 20, 2, 0)
4	0	0	0	-5	0	(25, 5, 0)	(0, 175, 285, 180, 50, 5, 0)
5	(5, 1, 0)	0	-(10, 2, 0)	(0, 10, 2, 0)	(25, 5, 0)	-(0, 50, 20, 2, 0)	-(160, 427, 649, 474, 172, 30, 2, 0)
6	(0, 35, 57, 36, 10, 1)	0	-(0, 70, 114, 72, 20, 2)	(32, 79, 114, 72, 20, 2)	(0, 175, 285, 180, 50, 5, 0)	-(160, 427, 649, 474, 172, 30, 2)	-(0, 2240, 6728, 11310, 12826)

$\frac{d_x=3}{d_y/d_z}$	0	1	2	3	4	5	6
0	0	0	0	0	1	(0, 4, 1, 0)	(9, 2, 0)
1	0	0	0	0	0	0	0
2	0	0	-1	(0, 1, 0)	(6, 1, 0)	-(0, 18, 8, 1)	-(45, 54, 59, 36, 10, 1)
3	0	0	(0, 1, 0)	-(0, 1, 0)	-(0, 6, 1, 0)	(0, 18, 8, 1, 0)	(0, 45, 54, 59, 36, 10, 1, 0)
4	-1	0	(6, 1, 0)	-(0, 6, 1, 0)	-(27, 9, 1, 0)	(0, 72, 45, 11, 1, 0)	(190, 324, 402, 275, 96, 16, 1, 0)
5	(0, 4, 1, 0)	0	-(0, 18, 8, 1, 0)	(0, 18, 8, 1, 0)	(0, 72, 45, 11, 1, 0)	-(0, 180, 168, 67, 13, 1, 0)	-(0, 490, 1072, 1470, 1168, 527, 134, 18, 1, 0)
6	(9, 2, 0)	0	-(45, 54, 59, 36, 10, 1)	(0, 45, 54, 59, 36, 10)	(190, 324, 402, 275, 96, 16)	-(0, 490, 1072, 1470, 1168, 527)	-(1314, 4297, 8082, 9600, 8269)

$\frac{d_x=4}{d_y/d_z}$	0	1	2	3	4	5	6
0	0	0	0	0	0	-1	0
1	0	0	0	0	0	0	0
2	0	0	0	-1	0	(11, 2, 0)	(0, 34, 57, 36, 10, 1, 0)
3	0	0	-1	(0, 1, 0)	4	-(0, 11, 2, 0)	-(35, 42, 57, 36, 10, 1, 0)
4	0	0	0	4	-(9, 6, 1, 0)	-(42, 19, 27, 9, 1, 0)	-(0, 82, 174, 126, 38, 4, 0)
5	-1	0	(11, 2, 0)	-(0, 11, 2, 0)	-(42, 19, 27, 9, 1, 0)	-(105, 41, 104, 54, 12, 1, 0)	(329, 356, 495, 402, 158, 29, 2, 0)
6	0	0	(0, 34, 57, 36, 10, 1)	-(35, 42, 57, 36, 10, 1)	-(0, 82, 174, 126, 38, 4)	(329, 356, 495, 402, 158, 29, 2)	(0, 2056, 5258, 7092, 6925, 5010)

$\frac{d_x=5}{d_y/d_z}$	0	1	2	3	4	5	6
0	0	0	0	0	0	0	-1
1	0	0	0	0	0	0	0
2	0	0	0	0	-1	(0, 5, 1)	(22, 8, 1)
3	0	0	0	0	(0, 1, 0)	-(0, 5, 1, 0)	-(0, 22, 8, 1)
4	0	0	1	(0, 1, 0)	(18, 7, 1, 0)	-(0, 60, 38)	-(192, 155, 88)
5	0	0	(0, 5, 1)	-(0, 5, 1, 0)	-(0, 60, 38)	(0, 186, 169)	(0, 570, 685)
6	1	0	(22, 8, 1)	-(0, 22, 8, 1)	-(192, 155, 88)	(0, 570, 685)	(1786, 3163)

$\frac{d_x=6}{d_y/d_z}$	0	1	2	3	4	5	6
0	0	0	0	0	0	0	0
1	0	0	0	0	0	0	0
2	0	0	0	0	0	-1	0
3	0	0	0	0	0	(0, 1)	6
4	0	0	0	0	0	(18, 3, 0)	-(0, 27, 26)
5	0	0	-1	(0, 1)	(18, 3, 0)	-(0, 60, 21, 2)	-(198, 24, -40)
6	0	0	0	6	-(0, 27, 26)	-(198, 24, -40)	(0, 36, -96, -88)

Table 4: ${}^B N_{d_x, d_y, d_z}^{(\chi)}$ for involution 2 of $[\mathbb{P}^2]^2$.

$\frac{d_x=0}{d_z/d_u}$	0	1	2	3
0	0	0	0	0
1	0	0	0	0
2	0	0	0	0
3	0	0	0	0
4	0	0	0	0
5	0	0	0	0
6	0	0	0	0

$\frac{d_x=1}{d_z/d_u}$	0	1	2	3
0	-1	1	0	0
1	-1	0	0	0
2	-1	1	0	0
3	-1	1	0	0
4	-1	1	0	0
5	-1	1	0	0
6	-1	1	0	0

$\frac{d_x=2}{d_z/d_u}$	0	1	2	3
0	0	0	0	0
1	0	0	0	0
2	0	0	0	0
3	(0, 1, 0)	-(0, 1, 0)	0	0
4	0	0	0	0
5	(0, 4, 1, 0)	-(0, 5, 1, 0)	(0, 1, 0)	0
6	0	0	0	0

$\frac{d_x=3}{d_z/d_u}$	0	1	2	3
0	0	0	1	-1
1	0	0	0	0
2	0	-1	2	-1
3	1	-2	2	0
4	2	-(6, 1, 0)	(6, 1, 0)	-2
5	(5, 1, 0)	-(11, 2, 0)	(8, 1, 0)	-2
6	(9, 2, 0)	-(22, 8, 1, 0)	(18, 7, 1, 0)	-(5, 1, 0)

$\frac{d_x=4}{d_z/d_u}$	0	1	2	3
0	0	0	(0, 1, 0)	-(0, 4, 1, 0)
1	0	0	0	0
2	0	0	0	-(0, 4, 1, 0)
3	0	(0, 1, 0)	-(0, 2, 0)	(0, 1, 0)
4	(0, 3, 1, 0)	0	-(0, 3, 1, 0)	0
5	-(0, 4, 1, 0)	(0, 18, 8, 1, 0)	-(0, 24, 9, 1, 0)	(0, 11, 2, 0)
6	(0, 35, 57, 36, 10, 1, 0)	-(0, 34, 57, 36, 10, 1, 0)	-(0, 9, 6, 1, 0)	(0, 8, 6, 1, 0)

$\frac{d_x=5}{d_z/d_u}$	0	1	2	3
0	0	0	0	(4, 4, 1, 0)
1	0	0	0	0
2	0	0	-1	(9, 5, 1, 0)
3	0	0	-3	(8, 4, 1, 0)
4	0	2	-(12, 2, 0)	(30, 13, 2, 0)
5	-(5, 10, 6, 1, 0)	(10, 2, 0)	(-24, 5, 6, 1, 0)	(39, 10, 1, 0)
6	-(14, 40, 57, 36, 10, 1, 0)	(45, 54, 59, 36, 10, 1, 0)	-(87, 37, 5, 0)	(115, 63, 14, 1, 0)

$\frac{d_x=6}{d_z/d_u}$	0	1	2	3
0	0	0	0	(0, 8, 2, 0)
1	0	0	0	0
2	0	0	0	(0, 8, 2, 0)
3	0	0	(0, 1, 0)	-(0, 9, 5, 1, 0)
4	0	0	0	-(0, -4, 3, 1, 0)
5	0	-(0, 4, 1, 0)	(0, 36, 16, 2, 0)	-(108, 76, 21, 2, 0)
6	-(44, 63, 37, 10, 1, 0)	(0, 70, 114, 72, 20, 2, 0)	-(0, 50, 102, 70, 20, 2, 0)	-(0, 30, 38, 12, 1, 0)

Table 5: $A_{d_x, d_z, d_u}^{(x)}$ for the involution of the hybridfly.

$\frac{d_x=0}{d_x/d_u}$	0	1	2	3
0	0	0	(0, 1, 0)	(0, 8, 2, 0)
1	-1	0	0	0
2	0	0	0	0
3	1	0	0	0
4	(0, 3, 1, 0)	0	0	0
5	-(5, 10, 6, 1, 0)	0	0	0
6	-(0, 44, 63, 37, 10, 1, 0)	0	0	0

$\frac{d_x=1}{d_x/d_u}$	0	1	2	3
0	1	1	1	(4, 4, 1, 0)
1	0	0	0	0
2	-1	-1	-1	-(4, 4, 1, 0)
3	(0, 1, 0)	(0, 1, 0)	(0, 1, 0)	(0, 4, 4, 1, 0)
4	2	2	2	(8, 8, 2, 0)
5	-(0, 4, 1, 0)	-(0, 4, 1, 0)	-(0, 4, 1, 0)	-(0, 16, 20, 8, 1, 0)
6	-(14, 40, 57, 36, 10, 1, 0)	-(14, 40, 57, 36, 10, 1, 0)	-(14, 40, 57, 36, 10, 1, 0)	-(56, 216, 402, 412, 241, 80)

$\frac{d_x=2}{d_x/d_u}$	0	1	2	3
0	0	0	0	-(0, 4, 1, 0)
1	0	0	0	0
2	0	0	0	(0, 8, 2, 0)
3	-1	-2	-3	-(10, 8, 2, 0)
4	0	0	0	-(0, 20, 5, 0)
5	(5, 1, 0)	(10, 2, 0)	(15, 3, 0)	(50, 50, 18, 2, 0)
6	(0, 35, 57, 36)	(0, 70, 114, 72, 20)	(105, 171, 108, 30)	(0, 478, 918, 895, 502)

$\frac{d_x=3}{d_x/d_u}$	0	1	2	3
0	0	0	0	-1
1	0	0	0	0
2	0	1	2	(9, 5, 1, 0)
3	0	-(0, 1, 0)	-(0, 2, 0)	-(0, 9, 5, 1, 0)
4	-1	-(6, 1, 0)	-(12, 2, 0)	-(46, 36, 11, 1, 0)
5	(0, 4, 1, 0)	(0, 18, 8, 1)	(0, 36, 16, 2)	(0, 130, 142, 64, 13, 1)
6	(9, 2, 0)	(45, 54, 59, 36, 10)	(90, 108, 118, 72, 20)	(334, 668, 840, 673, 329)

$\frac{d_x=4}{d_x/d_u}$	0	1	2	3
0	0	0	0	0
1	0	0	0	0
2	0	0	0	-(0, 4, 1, 0)
3	0	1	2	(8, 4, 1, 0)
4	0	0	-(0, 3, 1, 0)	-(0, -4, 3, 1, 0)
5	-1	-(11, 2, 0)	(-24, 5, 6, 1, 0)	(-88, -24, 14, 8, 1, 0)
6	0	-(34, 57, 36, 10, 1, 0)	-(0, 50, 102, 70, 20, 2, 0)	-(0, 340, 593, 538, 279, 84, 14, 1)

$\frac{d_x=5}{d_x/d_u}$	0	1	2	3
0	0	0	0	0
1	0	0	0	0
2	0	0	0	-1
3	0	0	0	(0, 1, 0)
4	0	1	(6, 1, 0)	(30, 13, 2, 0)
5	0	-(0, 5, 1, 0)	-(0, 24, 9, 1, 0)	-(0, 108, 76, 21, 2, 0)
6	-1	-(22, 8, 1, 0)	-(87, 37, 5, 0)	-(366, 317, 152, 51, 11, 1, 0)

$\frac{d_x=6}{d_x/d_u}$	0	1	2	3
0	0	0	0	0
1	0	0	0	0
2	0	0	0	0
3	0	0	0	0
4	0	0	0	0
5	0	1	(8, 1, 0)	(39, 10, 1, 0)
6	0	0	-(9, 6, 1, 0)	-(0, 30, 38, 12, 1, 0)

Table 6: $B N_{d_x, d_z, d_u}^{(x)}$ for the involution of $[\mathbb{F}_0][\mathbb{P}^2]$.

$d_x=0$ d_y/d_z	0	1	2	3
0	0	0	0	0
1	0	0	0	0
2	0	0	0	0
3	0	0	0	0

$d_x=1$ d_y/d_z	0	1	2	3
0	-1	1	0	0
1	1	-1	0	0
2	0	0	0	0
3	0	0	0	0

$d_x=2$ d_y/d_z	0	1	2	3
0	0	0	0	0
1	0	0	0	0
2	0	0	0	0
3	0	0	0	0

$d_x=3$ d_y/d_z	0	1	2	3
0	0	0	0	0
1	0	3	-3	0
2	0	-3	3	0
3	0	0	0	0

$d_x=4$ d_y/d_z	0	1	2	3
0	0	0	0	0
1	0	0	0	0
2	0	0	(0, 1, 0)	0
3	0	0	0	0

$d_x=5$ d_y/d_z	0	1	2	3
0	0	0	0	0
1	0	0	5	-5
2	0	5	-(30, 6, 0)	(30, 6, 0)
3	0	-5	(30, 6, 0)	-(30, 6, 0)

$d_x=6$ d_y/d_z	0	1	2	3
0	0	0	0	0
1	0	0	0	0
2	0	0	0	(0, 4, 1, 0)
3	0	0	(0, 4, 1, 0)	-(0, 8, 2, 0)

Table 7: $AN_{d_x, d_y, d_z}^{(\chi)}$ for involution 1 & 3 of the pentafly. Note that involution 3 has additional non-vanishing invariants that do not satisfy the d_Q - χ -correlation implicit in these tables. Namely, the additional invariants are $AN_{0,1,0}^{(-1)} = -AN_{0,0,1}^{(-1)} = 1$.

$d_x=0$ d_y/d_z	0	1	2	3
0	0	0	0	0
1	0	0	0	0
2	0	0	0	0
3	0	0	0	0

$d_x=1$ d_y/d_z	0	1	2	3
0	1	1	0	0
1	1	3	5	7
2	0	5	(35, 8, 0)	(135, 72, 11, 0)
3	0	7	(135, 72, 11, 0)	(1100, 1304, 662, 160, 15, 0)

$d_x=2$ d_y/d_z	0	1	2	3
0	0	0	0	0
1	0	0	0	0
2	0	0	0	0
3	0	0	0	0

$d_x=3$ d_y/d_z	0	1	2	3
0	0	0	0	0
1	0	-1	-3	-5
2	0	-3	-(30, 6, 0)	-(147, 66, 9, 0)
3	0	-5	-(174, 66, 9, 0)	-(1494, 1509, 681, 150, 13, 0)

$d_x=4$ d_y/d_z	0	1	2	3
0	0	0	0	0
1	0	0	0	0
2	0	0	(0, 1, 0)	(0, 4, 1, 0)
3	0	0	(0, 4, 1, 0)	(0, 40, 30, 9, 1, 0)

$d_x=5$ d_y/d_z	0	1	2	3
0	0	0	0	0
1	0	0	0	0
2	0	0	3	(30, 6, 0)
3	0	0	(30, 6, 0)	(504, 341, 95, 10, 0)

$d_x=2$ d_y/d_z	0	1	2	3
0	0	0	0	0
1	0	0	0	0
2	0	0	0	0
3	0	0	0	-(8, 2, 0)

Table 8: $BN_{d_x, d_y, d_z}^{(\chi)}$ for involution 1 & 3 of $[\mathbb{F}_0]^2$. Note that involution 3 has additional non-vanishing invariants that do not satisfy the d_Q - χ -correlation implicit in these tables. Namely, the additional invariants are $BN_{2,1,0}^{(-1)} = -BN_{2,0,1}^{(-1)} = 1$.

$d_x=0$ d_y/d_z	0	1	2	3
0	0	0	0	0
1	0	0	0	0
2	0	0	0	0
3	0	0	0	0

$d_x=1$ d_y/d_z	0	1	2	3
0	-1	1	0	0
1	1	-1	0	0
2	0	0	0	0
3	0	0	0	0

$d_x=2$ d_y/d_z	0	1	2	3
0	0	0	0	0
1	0	0	0	0
2	0	0	0	0
3	0	0	0	0

$d_x=3$ d_y/d_z	0	1	2	3
0	0	0	1	-1
1	0	1	-2	1
2	1	-2	1	0
3	-1	1	0	0

$d_x=4$ d_y/d_z	0	1	2	3
0	0	0	(0, 1, 0)	-(0, 4, 1, 0)
1	0	0	0	(0, 4, 1, 0)
2	(0, 1, 0)	0	-(0, 1, 0)	0
3	-(0, 4, 1, 0)	(0, 4, 1, 0)	0	0

$d_x=5$ d_y/d_z	0	1	2	3
0	0	0	0	(4, 4, 1, 0)
1	0	0	1	-(9, 5, 1, 0)
2	0	1	-4	(8, 1, 0)
3	(4, 4, 1, 0)	-(9, 5, 1, 0)	(8, 1, 0)	-4

$d_x=6$ d_y/d_z	0	1	2	3
0	0	0	0	(0, 8, 2, 0)
1	0	0	0	-(0, 8, 2, 0)
2	0	0	0	(0, 4, 1, 0)
3	(0, 8, 2, 0)	-(0, 8, 2, 0)	(0, 4, 1, 0)	0

Table 9: $^A N_{d_x, d_z, d_u}^{(x)}$ for involution 2 of the pentafly.

$d_x=0$ d_y/d_z	0	1	2	3
0	0	0	(0, 1, 0)	(0, 8, 2, 0)
1	0	0	0	0
2	(0, 1, 0)	0	0	0
3	(0, 8, 2, 0)	0	0	0

$d_x=1$ d_y/d_z	0	1	2	3
0	1	1	1	(4, 4, 1, 0)
1	1	1	1	(4, 4, 1, 0)
2	1	1	1	(4, 4, 1, 0)
3	(4, 4, 1, 0)	(4, 4, 1, 0)	(4, 4, 1, 0)	(16, 32, 24, 8, 1, 0)

$d_x=2$ d_y/d_z	0	1	2	3
0	0	0	0	-(0, 4, 1, 0)
1	0	0	0	-(0, 8, 2, 0)
2	0	0	0	-(0, 12, 3, 0)
3	-(0, 4, 1, 0)	-(0, 8, 2, 0)	-(0, 12, 3, 0)	-(0, 80, 52, 16, 2, 0)

$d_x=3$ d_y/d_z	0	1	2	3
0	0	0	0	-1
1	0	-1	-2	-(9, 5, 1, 0)
2	0	-2	-4	-(18, 10, 2, 0)
3	-1	-(9, 5, 1, 0)	-(18, 10, 2, 0)	-(74, 87, 43, 10, 1, 0)

$d_x=4$ d_y/d_z	0	1	2	3
0	0	0	0	0
1	0	0	0	(0, 4, 1, 0)
2	0	0	-1	(0, 4, 1, 0)
3	0	(0, 4, 1, 0)	(0, 4, 1, 0)	(0, 48, 24, 7, 1, 0)

$d_x=5$ d_y/d_z	0	1	2	3
0	0	0	0	0
1	0	0	0	1
2	0	0	1	(8, 1, 0)
3	0	1	(8, 1, 0)	(46, 19, 3, 0)

$d_x=6$ d_y/d_z	0	1	2	3
0	0	0	0	0
1	0	0	0	0
2	0	0	0	0
3	0	0	0	0

Table 10: $^B N_{d_x, d_y, d_z}^{(x)}$ for involution 2 of $[\mathbb{F}_0]^2$.

References

- [1] M. Aganagic, A. Klemm, M. Marino and C. Vafa, “The topological vertex,” *Commun. Math. Phys.* **254** (2005) 425 [arXiv:hep-th/0305132].
- [2] D. Krefl and J. Walcher, “The Real Topological String on a local Calabi-Yau,” arXiv:0902.0616 [hep-th].
- [3] J. Walcher, “Evidence for Tadpole Cancellation in the Topological String,” *Comm. Number Th. Phys.* **3** 111–172 (2009) [arXiv:0712.2775 [hep-th]].
- [4] V. Bouchard, B. Florea and M. Marino, “Counting higher genus curves with crosscaps in Calabi-Yau orientifolds,” *JHEP* **0412** (2004) 035 [arXiv:hep-th/0405083].
- [5] V. Bouchard, B. Florea and M. Marino, “Topological open string amplitudes on orientifolds,” *JHEP* **0502** (2005) 002 [arXiv:hep-th/0411227].
- [6] P. L. H. Cook, H. Ooguri and J. Yang, “New Anomalies in Topological String Theory,” *Prog. Theor. Phys. Suppl.* **177** (2009) 120 [arXiv:0804.1120 [hep-th]].
- [7] G. Bonelli, A. Prudenziati, A. Tanzini and J. Yang, “Decoupling A and B model in open string theory – Topological adventures in the world of tadpoles,” *JHEP* **0906** (2009) 046 [arXiv:0905.1286 [hep-th]].
- [8] P. Horava, “Chern-Simons gauge theory on orbifolds: Open strings from three dimensions,” *J. Geom. Phys.* **21**, 1 (1996) [arXiv:hep-th/9404101].
- [9] A. Okounkov, N. Reshetikhin and C. Vafa, “Quantum Calabi-Yau and classical crystals,” arXiv:hep-th/0309208.
- [10] K. Hori, K. Hosomichi, D. C. Page, R. Rabadan and J. Walcher, “Non-perturbative orientifold transitions at the conifold,” *JHEP* **0510**, 026 (2005) [arXiv:hep-th/0506234].
- [11] R. Gopakumar and C. Vafa, “M-theory and topological strings. I,” arXiv:hep-th/9809187.
- [12] I. G. Macdonald, “Symmetric Functions and Hall Polynomials,” Oxford University Press (1995)
- [13] S. Sinha and C. Vafa, “SO and Sp Chern-Simons at large N,” arXiv:hep-th/0012136.
- [14] E. Witten, “Chern-Simons Gauge Theory As A String Theory,” *Prog. Math.* **133**, 637 (1995) [arXiv:hep-th/9207094].
- [15] P. A. MacMahon, “Partitions of numbers whose graphs possess symmetry,” *Trans. Cambridge Phil. Soc.* **17** 149–170 (1898–99)
- [16] G. Andrews, “Plane partitions (I): the MacMahon conjecture,” *Studies in Foundations and Combinatorics, Advances in Mathematics Supplementary Studies* **1**, 131–150 (1978)
- [17] V. Kac, “Vertex Algebras for Beginners,” (University Lecture Series, No. 10) American Mathematical Society (1997)
- [18] C. Faber and R. Pandharipande, “Hodge integrals and Gromov-Witten theory,” *Invent. Maht.* **139**, 173 (2000) arXiv:math.ag/9810173

- [19] A. Dabholkar, F. Denef, G. W. Moore and B. Pioline, “Precision counting of small black holes,” *JHEP* **0510**, 096 (2005) [arXiv:hep-th/0507014].
- [20] S. Pasquetti and R. Schiappa, “Borel and Stokes Nonperturbative Phenomena in Topological String Theory and $c=1$ Matrix Models,” arXiv:0907.4082 [hep-th].
- [21] M. Bershadsky, S. Cecotti, H. Ooguri and C. Vafa, “Holomorphic anomalies in topological field theories,” *Nucl. Phys. B* **405**, 279 (1993) [arXiv:hep-th/9302103].
- [22] H. Ooguri and C. Vafa, “Knot invariants and topological strings,” *Nucl. Phys. B* **577**, 419 (2000) [arXiv:hep-th/9912123].
- [23] T. M. Chiang, A. Klemm, S. T. Yau and E. Zaslow, “Local mirror symmetry: Calculations and interpretations,” *Adv. Theor. Math. Phys.* **3** (1999) 495 [arXiv:hep-th/9903053].
- [24] Y. Konishi and S. Minabe, “Flop invariance of the topological vertex,” arXiv:math/0601352.
- [25] S. H. Katz, A. Klemm and C. Vafa, *Adv. Theor. Math. Phys.* **3**, 1445 (1999) [arXiv:hep-th/9910181].
- [26] J. Bryan and D. Karp, “The closed topological vertex via the Cremona transform,” *J. Algebraic Geometry*, **14**, 529–542, [arXiv:math.ag/0311208]